

AD-A101 417

CATHOLIC UNIV OF AMERICA WASHINGTON DC VITREOUS STATE LAB F/8 7/4
THE COMMINUTION BEHAVIOR OF LIQUIDS. (U)
JUN 81 T A LITOVITZ, C J MONTROSE

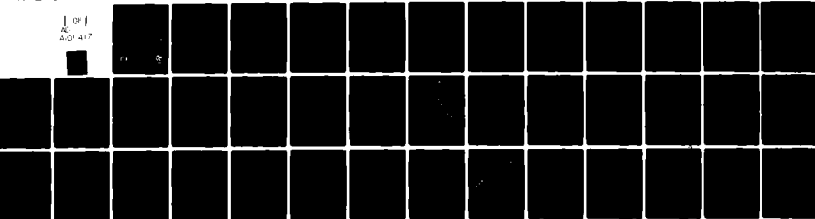
DAA629-76-D-0100

NL

UNCLASSIFIED

ARCSL-CR-81025

1 OF 1
AC
AD-A101



END
DATE 8-8-81
8-8-81
DTIC

(12)

LEVEL II

AD

CHEMICAL SYSTEMS LABORATORY CONTRACTOR REPORT

ARCSL-CR-81025

AD A 101417

THE COMMINUTION BEHAVIOR OF LIQUIDS

Final Report

by

T. A. Litovitz
C. J. Montrose

June 1981

DTIC
ELECTED
S JUL 15 1981 D
B

CATHOLIC UNIVERSITY OF AMERICA
Vitreous State Laboratory
Washington, D.C. 20064

Contract DAAG29-76-D0100 ✓

DTIC FILE COPY



US ARMY ARMAMENT RESEARCH AND DEVELOPMENT COMMAND
Chemical Systems Laboratory
Aberdeen Proving Ground, Maryland 21010



Approved for public release; distribution unlimited.

(12)

LEVEL II

AD

CHEMICAL SYSTEMS LABORATORY CONTRACTOR REPORT

ARCSL-CR-81025

AD A 101417

THE COMMINUTION BEHAVIOR OF LIQUIDS

Final Report

by

T. A. Litovitz
C. J. Montrose

June 1981

DTIC
ELECTED
S JUL 15 1981 D
B

CATHOLIC UNIVERSITY OF AMERICA
Vitreous State Laboratory
Washington, D.C. 20064

Contract DAAG29-76-D0100 ✓

DTIC FILE COPY



US ARMY ARMAMENT RESEARCH AND DEVELOPMENT COMMAND
Chemical Systems Laboratory
Aberdeen Proving Ground, Maryland 21010



Approved for public release; distribution unlimited.

Disclaimer

The views, opinions, and/or findings contained in this report are those of the authors and should not be construed as an official Department of the Army position, policy, or decision unless so designated by other documentation.

Disposition

Destroy this report when it is no longer needed. Do not return it to the originator.

Disclaimer

The views, opinions, and/or findings contained in this report are those of the authors and should not be construed as an official Department of the Army position, policy, or decision unless so designated by other documentation.

Disposition

Destroy this report when it is no longer needed. Do not return it to the originator.

UNCLASSIFIED

SECURITY CLASSIFICATION OF THIS PAGE (When Data Entered)

REPORT DOCUMENTATION PAGE		READ INSTRUCTIONS BEFORE COMPLETING FORM	
1. REPORT NUMBER ARCS-CCR-81025	2. GOVT ACCESSION NO. AD-A101417	3. RECIPIENT'S CATALOG NUMBER 9 rept.	
4. TITLE (and Subtitle) THE COMMINUTION BEHAVIOR OF LIQUIDS		5. TYPE OF REPORT & PERIOD COVERED Final, Sep 1979 - March 1980	
6. AUTHOR(s) T. A. Litovitz C. J. Montrose		7. CONTRACT OR GRANT NUMBER(s) DAAG29-76-D-0100 D.O. 1438	
8. PERFORMING ORGANIZATION NAME AND ADDRESS Catholic University of America Vitreous State Laboratory Washington, D.C. 20064		9. PROGRAM ELEMENT, PROJECT, TASK AREA & WORK UNIT NUMBERS 11	
10. CONTROLLING OFFICE NAME AND ADDRESS Commander/Director, Chemical Systems Laboratory ATTN: DRDAR-CLJ-R Aberdeen Proving Ground, MD 21010		12. REPORT DATE June 1981	
13. NUMBER OF PAGES 42		14. SECURITY CLASS. (of this report) UNCLASSIFIED	
15. DECLASSIFICATION/DOWNGRADING SCHEDULE NA		16. DISTRIBUTION STATEMENT (of this Report) Approved for public release; distribution unlimited. 16 1L 16110-A71A	
17. DISTRIBUTION STATEMENT (of the abstract entered in Block 20, if different from Report)			
18. SUPPLEMENTARY NOTES Contract Project Officer: Arthur K. Stuemple (DRDAR-CLB-PO, 301-671-3058)			
19. KEY WORDS (Continue on reverse side if necessary and identify by block number) Explosive dissemination Computer simulation Dissemination Molecular dynamics Drops			
20. ABSTRACT (Continue on reverse side if necessary and identify by block number) A physical model of the explosive comminution process in liquids is presented. The key feature of the model involves the development of flaws in the liquid under the action of large explosively generated stresses. It is at these flaws that the material fails via a process termed "liquid fracture." Guided by molecular dynamics (MD) studies, a highly simplified view of the process is proposed. Even this simplified picture is relatively successful in yielding semiquantitative agreement with experimental data.			

DD FORM 1473 EDITION OF 1 NOV 65 IS OBSOLETE

UNCLASSIFIED

SECURITY CLASSIFICATION OF THIS PAGE (When Data Entered)

1/2

404951

UNCLASSIFIED

SECURITY CLASSIFICATION OF THIS PAGE (When Data Entered)

REPORT DOCUMENTATION PAGE		READ INSTRUCTIONS BEFORE COMPLETING FORM	
1. REPORT NUMBER ARCS-HCR-81025	2. GOVT ACCESSION NO. AD-A101417	3. RECIPIENT'S CATALOG NUMBER 9 rept.	
4. TITLE (and Subtitle) THE COMMINUTION BEHAVIOR OF LIQUIDS		5. TYPE OF REPORT & PERIOD COVERED Final, Sep 1979 - March 1980	
6. AUTHOR(s) T. A. Litovitz C. J. Montrose		7. CONTRACT OR GRANT NUMBER(s) DAAG29-76-D-0100 D.O. 1438	
8. PERFORMING ORGANIZATION NAME AND ADDRESS Catholic University of America Vitreous State Laboratory Washington, D.C. 20064		9. PROGRAM ELEMENT, PROJECT, TASK AREA & WORK UNIT NUMBERS 11	
10. CONTROLLING OFFICE NAME AND ADDRESS Commander/Director, Chemical Systems Laboratory ATTN: DRDAR-CLJ-R Aberdeen Proving Ground, MD 21010		12. REPORT DATE June 1981	
13. NUMBER OF PAGES 42		14. SECURITY CLASS. (of this report) UNCLASSIFIED	
15. DECLASSIFICATION/DOWNGRADING SCHEDULE NA		16. DISTRIBUTION STATEMENT (of this Report) Approved for public release; distribution unlimited. 16 1L 16110-A71A	
17. DISTRIBUTION STATEMENT (of the abstract entered in Block 20, if different from Report)			
18. SUPPLEMENTARY NOTES Contract Project Officer: Arthur K. Stuemple (DRDAR-CLB-PO, 301-671-3058)			
19. KEY WORDS (Continue on reverse side if necessary and identify by block number) Explosive dissemination Computer simulation Dissemination Molecular dynamics Drops			
20. ABSTRACT (Continue on reverse side if necessary and identify by block number) A physical model of the explosive comminution process in liquids is presented. The key feature of the model involves the development of flaws in the liquid under the action of large explosively generated stresses. It is at these flaws that the material fails via a process termed "liquid fracture." Guided by molecular dynamics (MD) studies, a highly simplified view of the process is proposed. Even this simplified picture is relatively successful in yielding semiquantitative agreement with experimental data.			

DD FORM 1 JAN 73 1473 EDITION OF 1 NOV 65 IS OBSOLETE

UNCLASSIFIED

SECURITY CLASSIFICATION OF THIS PAGE (When Data Entered)

1/2

404951

PREFACE

The research described in this report was authorized by contract 1L161102A71A, Research in Defense Systems, Technical Area - Chemical Defense Research. This work was started in September 1979 and completed in March 1980.

Reproduction of this document in whole or in part is prohibited except with permission of the Commander/Director, Chemical Systems Laboratory, ATTN: DRDAR-CLJ-R, Aberdeen Proving Ground, MD 21010. However, Defense Technical Information Center and the National Technical Information Service are authorized to reproduce the document for US Government purposes.

Accession For	
NTIS	100-1
DTIC	100
Urgency	
Janitor	
By	
Distr	
Avail	100-10
Year	1980
Dist	
A	

PREFACE

The research described in this report was authorized by contract 1L161102A71A, Research in Defense Systems, Technical Area - Chemical Defense Research. This work was started in September 1979 and completed in March 1980.

Reproduction of this document in whole or in part is prohibited except with permission of the Commander/Director, Chemical Systems Laboratory, ATTN: DRDAR-CLJ-R, Aberdeen Proving Ground, MD 21010. However, Defense Technical Information Center and the National Technical Information Service are authorized to reproduce the document for US Government purposes.

Accession For	
NTIS	100-1
DTIC	100
Urgency	
Janitor	
By	
Distr	
Avail	100-10
Year	1980
Dist	
A	

TABLE OF CONTENTS

	Page
1 INTRODUCTION	7
2 BACKGROUND	7
3 PRELIMINARY CONSIDERATIONS	8
4 A PHYSICAL MODEL FOR COMMINUTION.....	9
5 COMPARISON WITH EXPERIMENT.....	13
6 THE EFFECT OF POLYMERIC ADDITIVES	15
7 SUMMARY AND CONCLUSIONS.....	15
APPENDIX	17
DISTRIBUTION LIST.....	39

TABLE OF CONTENTS

	Page
1 INTRODUCTION	7
2 BACKGROUND	7
3 PRELIMINARY CONSIDERATIONS	8
4 A PHYSICAL MODEL FOR COMMINUTION.....	9
5 COMPARISON WITH EXPERIMENT.....	13
6 THE EFFECT OF POLYMERIC ADDITIVES	15
7 SUMMARY AND CONCLUSIONS.....	15
APPENDIX	17
DISTRIBUTION LIST.....	39

THE COMMINUTION BEHAVIOR OF LIQUIDS

1. INTRODUCTION

The aim of this investigation is to assess the role of nonlinear viscoelasticity in the process of liquid comminution under explosive stress. Ultimately the goal of the program is to evaluate the hypothesis that the crucial factor in determining the comminution and dispersal characteristics of liquids under these conditions is the nonlinear dynamical response behavior of the liquids. In attacking the problem, it is essential first to develop a model of comminution that incorporates the mechanism of liquid response and failure when subjected to explosively generated stresses. The central theme of this report is the proposal of such a model, the exploration of its consequences, and, where possible, a comparison of predictions based upon it with experimental data. This model calculation forms the first part of the report. Following this is a brief section which isolates those elements of the proposed mechanism that are controlled by the nonlinear viscoelastic characteristics of the liquid. Lastly we address the issue of utilizing computer-simulation molecular-dynamics (MD) experiments as a tool for probing these nonlinear characteristics; we conclude that MD experiments offer significant potential for contributing to the understanding and control of the processes of explosive liquid comminution and dispersal.

2. BACKGROUND

The experimental study that provides the principal impetus and guidance for addressing comminution behavior is that of Gerber and Stuempfle.* In this work a high-explosive projector was employed to produce dissemination of a liquid cloud around a preferential vertical axis. A three-dimensional sampling array was used to measure the mass distribution of the cloud following its emergence from the projector. The mass distribution along the vertical z-axis was described by a Weibull distribution,

$$f(z) = (\beta/z)(z/z_0)^\beta \exp[-(z/z_0)^\beta]$$

such that $f(z)dz$ gives the mass fraction lost in the height range z to $z + dz$ above the projector. In the Weibull form z_0 is a characteristic length parameter and β is a shape parameter. Gerber and Stuempfle present their data in terms of four parameters z_{50} — the median of the distribution — and the first three moments of the distribution. In terms of the parameters of the distribution

$$z_{50} = z_0 (\ell \eta 2)^{1/\beta},$$

and the mean or first moment is

$$\langle z \rangle = z_0 \Gamma(1/\beta)/\beta.$$

Values of β fall in the range from about 0.6 to 3 with most of the more than 30 liquids studied being described by β 's near 2; $\langle z \rangle$ values varied from about 65cm to about 335cm. Generally one finds that larger values of $\langle z \rangle$ are accompanied by larger values of β . A major theme in what follows is the attempt to understand those liquid properties that are operative in the

* Gerber, B.V. and Stuempfle, A.D. TSD 004.7-11/Vol. 1. A New Experimental Technique for Studying the Explosive Comminution of Liquids. 1976 Army Science Conference Proceedings. Vol. 1. September 1976. Unclassified Report.

THE COMMINUTION BEHAVIOR OF LIQUIDS

1. INTRODUCTION

The aim of this investigation is to assess the role of nonlinear viscoelasticity in the process of liquid comminution under explosive stress. Ultimately the goal of the program is to evaluate the hypothesis that the crucial factor in determining the comminution and dispersal characteristics of liquids under these conditions is the nonlinear dynamical response behavior of the liquids. In attacking the problem, it is essential first to develop a model of comminution that incorporates the mechanism of liquid response and failure when subjected to explosively generated stresses. The central theme of this report is the proposal of such a model, the exploration of its consequences, and, where possible, a comparison of predictions based upon it with experimental data. This model calculation forms the first part of the report. Following this is a brief section which isolates those elements of the proposed mechanism that are controlled by the nonlinear viscoelastic characteristics of the liquid. Lastly we address the issue of utilizing computer-simulation molecular-dynamics (MD) experiments as a tool for probing these nonlinear characteristics; we conclude that MD experiments offer significant potential for contributing to the understanding and control of the processes of explosive liquid comminution and dispersal.

2. BACKGROUND

The experimental study that provides the principal impetus and guidance for addressing comminution behavior is that of Gerber and Stuempfle.* In this work a high-explosive projector was employed to produce dissemination of a liquid cloud around a preferential vertical axis. A three-dimensional sampling array was used to measure the mass distribution of the cloud following its emergence from the projector. The mass distribution along the vertical z-axis was described by a Weibull distribution,

$$f(z) = (\beta/z)(z/z_0)^\beta \exp[-(z/z_0)^\beta]$$

such that $f(z)dz$ gives the mass fraction lost in the height range z to $z + dz$ above the projector. In the Weibull form z_0 is a characteristic length parameter and β is a shape parameter. Gerber and Stuempfle present their data in terms of four parameters z_{50} — the median of the distribution — and the first three moments of the distribution. In terms of the parameters of the distribution

$$z_{50} = z_0 (\ell \eta 2)^{1/\beta},$$

and the mean or first moment is

$$\langle z \rangle = z_0 \Gamma(1/\beta)/\beta.$$

Values of β fall in the range from about 0.6 to 3 with most of the more than 30 liquids studied being described by β 's near 2; $\langle z \rangle$ values varied from about 65cm to about 335cm. Generally one finds that larger values of $\langle z \rangle$ are accompanied by larger values of β . A major theme in what follows is the attempt to understand those liquid properties that are operative in the

* Gerber, B.V. and Stuempfle, A.D. TSD 004.7-11/Vol. 1. A New Experimental Technique for Studying the Explosive Comminution of Liquids. 1976 Army Science Conference Proceedings. Vol. 1. September 1976. Unclassified Report.

determination of the average height $\langle z \rangle$. Exploring the details of the mass distribution pattern is beyond the scope of this work.

3. PRELIMINARY CONSIDERATIONS

In this section we give a crude description of the liquid comminution process. The principal result of the section is an equation giving the average height $\langle z \rangle$ in terms of the size of the particles or droplets that compose the cloud.

We consider the effect of the explosion on the liquid to be roughly separable into two major components:

(a) The explosive release of energy generates a shock wave that in passing through the liquid produces large tensile, compressional, and shear stresses. These cause local internal fissures within the liquid so that it comminutes into many small liquid fragments.

(b) The explosion produces a rapidly expanding gas that intrudes itself into the stress-produced fissures, thereby preventing their healing, and causing the liquid fragments to be expelled from the projector with a vertical velocity v_0 .

The dependence of the initial velocity on liquid parameters can be estimated by the following sort of rough argument. We shall assume that relatively little of the energy of explosion is used in the formation of the droplets so that most of the energy E is transferred to the kinetic energy of the droplets. The initial velocity imparted to the droplets then becomes

$$v_0 = (2E/m)^{1/2} \times \rho^{-1/2} \quad (1)$$

where m is the mass of a droplet, ϵ is the kinetic energy per droplet, and ρ is the liquid density. Assuming that E is the same for each explosion, it follows that the initial velocity of the droplets is dependent only on the density of the liquid.

The dynamical problem for the projected droplets can now be worked out straightforwardly, at least in lowest order approximation. We assume that the droplets are spherical and that the size distribution is characterized by a function $f(a)$ which gives the probability of a droplet's radius falling in the range a to $a+da$. We take the forces acting on a droplet of radius a to be

and (a) gravity: $-\frac{4}{3}\pi a^3 \rho g$,

(b) air resistance: $-6\pi\eta av$.

In these expressions g is the acceleration due to gravity, η is the viscosity of the medium (air) into which the droplet cloud is projected, and v is the instantaneous droplet velocity in the vertical direction. Newton's law then takes the form

$$\frac{dv}{dt} + v/\tau = -g, \quad (2)$$

where for a droplet of radius a

$$\tau = 2\rho a^2 / 9\eta. \quad (3)$$

determination of the average height $\langle z \rangle$. Exploring the details of the mass distribution pattern is beyond the scope of this work.

3. PRELIMINARY CONSIDERATIONS

In this section we give a crude description of the liquid comminution process. The principal result of the section is an equation giving the average height $\langle z \rangle$ in terms of the size of the particles or droplets that compose the cloud.

We consider the effect of the explosion on the liquid to be roughly separable into two major components:

(a) The explosive release of energy generates a shock wave that in passing through the liquid produces large tensile, compressional, and shear stresses. These cause local internal fissures within the liquid so that it comminutes into many small liquid fragments.

(b) The explosion produces a rapidly expanding gas that intrudes itself into the stress-produced fissures, thereby preventing their healing, and causing the liquid fragments to be expelled from the projector with a vertical velocity v_0 .

The dependence of the initial velocity on liquid parameters can be estimated by the following sort of rough argument. We shall assume that relatively little of the energy of explosion is used in the formation of the droplets so that most of the energy E is transferred to the kinetic energy of the droplets. The initial velocity imparted to the droplets then becomes

$$v_0 = (2E/m)^{1/2} \times \rho^{-1/2} \quad (1)$$

where m is the mass of a droplet, ϵ is the kinetic energy per droplet, and ρ is the liquid density. Assuming that E is the same for each explosion, it follows that the initial velocity of the droplets is dependent only on the density of the liquid.

The dynamical problem for the projected droplets can now be worked out straightforwardly, at least in lowest order approximation. We assume that the droplets are spherical and that the size distribution is characterized by a function $f(a)$ which gives the probability of a droplet's radius falling in the range a to $a+da$. We take the forces acting on a droplet of radius a to be

and (a) gravity: $-\frac{4}{3}\pi a^3 \rho g$,

(b) air resistance: $-6\pi\eta av$.

In these expressions g is the acceleration due to gravity, η is the viscosity of the medium (air) into which the droplet cloud is projected, and v is the instantaneous droplet velocity in the vertical direction. Newton's law then takes the form

$$\frac{dv}{dt} + v/\tau = -g, \quad (2)$$

where for a droplet of radius a

$$\tau = 2\rho a^2 / 9\eta. \quad (3)$$

The solution of (2) is just

$$v = v_0 \exp(-t/\tau) - g\tau [1 - \exp(-t/\tau)]. \quad (4)$$

Integrating this again gives the equation of motion

$$z(t) = v_0\tau [1 - \exp(-t/\tau)] + g\tau^2 1 - \frac{t}{\tau} \exp(-t/\tau). \quad (5)$$

The height to which a droplet rises, z , can then be found by setting $v=0$ in (4) and solving for the time:

$$t_0 = \tau \ln(1 + v_0/g\tau) \quad (6)$$

Putting $z = z(t_0)$ gives

$$z = v_0\tau - g\tau^2 \ln(1 + v_0/g\tau). \quad (7)$$

For typical values of η , ρ , and a ($\eta = 0.18 \text{ mP}$, $\rho \approx 1.3 \text{ g/cm}^3$, $a \approx 25 \mu\text{m}$), $\tau \approx .01 \text{ sec}$. Using $v_0 \approx 3 \times 10^4 \text{ cm/sec}$ and $g = 980 \text{ cm/sec}^2$ one gets $t_0 \approx .08 \text{ sec}$, which is of the correct order of magnitude to what is experimentally observed. Moreover $v_0 \gg g\tau$ so that approximately

$$z \approx v_0\tau. \quad (8)$$

Equation (8) is accurate to better than a percent or so for the full range of liquids and experimental conditions studied by Gerber and Stuempfle. Using equation (3) and averaging gives

$$\langle z \rangle = (2v_0/9\eta)\rho \langle a^2 \rangle, \quad (9)$$

where $\langle a^2 \rangle$ is the mean square droplet radius.

4. A PHYSICAL MODEL FOR COMMINUTION

The central issue is clear from equation (9): What are the processes - and thus the liquid characteristics - that determine the mean square droplet size? We assume that the mechanism of droplet formation is mainly a mechanical (as opposed to a thermal) one. At any instant even an equilibrium liquid exhibits local deviations from homogeneity and isotropy. One characterization of the deviations from homogeneity is the distribution of fluctuations in the density. From classical statistical mechanics the probability of occurrence of a density fluctuation in the range $\Delta\rho$ to $\Delta\rho + d\rho$ is

$$P(\Delta\rho)d\rho = (2\pi \langle \Delta\rho^2 \rangle)^{-1/2} \exp[-\Delta\rho^2/2\langle \Delta\rho^2 \rangle] d\rho, \quad (10)$$

where $\langle \Delta\rho^2 \rangle$ is the mean square density fluctuation given by

$$\langle \Delta\rho^2 \rangle = \rho^2 (kT/V)/K, \quad (11)$$

where T and ρ are the temperature and average density of the system, V is the volume of the region under consideration, k is Boltzmann's constant, and K is the equilibrium bulk modulus of the material.

We suggest that under the influence of the large explosively generated stresses, these local inhomogeneities will behave as structural flaws in the material: shear stresses tend to

The solution of (2) is just

$$v = v_0 \exp(-t/\tau) - g\tau [1 - \exp(-t/\tau)]. \quad (4)$$

Integrating this again gives the equation of motion

$$z(t) = v_0\tau [1 - \exp(-t/\tau)] + g\tau^2 1 - \frac{t}{\tau} \exp(-t/\tau). \quad (5)$$

The height to which a droplet rises, z , can then be found by setting $v=0$ in (4) and solving for the time:

$$t_0 = \tau \ln(1 + v_0/g\tau) \quad (6)$$

Putting $z = z(t_0)$ gives

$$z = v_0\tau - g\tau^2 \ln(1 + v_0/g\tau). \quad (7)$$

For typical values of η , ρ , and a ($\eta = 0.18 \text{ mP}$, $\rho \approx 1.3 \text{ g/cm}^3$, $a \approx 25 \mu\text{m}$), $\tau \approx .01 \text{ sec}$. Using $v_0 \approx 3 \times 10^4 \text{ cm/sec}$ and $g = 980 \text{ cm/sec}^2$ one gets $t_0 \approx .08 \text{ sec}$, which is of the correct order of magnitude to what is experimentally observed. Moreover $v_0 \gg g\tau$ so that approximately

$$z \approx v_0\tau. \quad (8)$$

Equation (8) is accurate to better than a percent or so for the full range of liquids and experimental conditions studied by Gerber and Stuempfle. Using equation (3) and averaging gives

$$\langle z \rangle = (2v_0/9\eta)\rho \langle a^2 \rangle, \quad (9)$$

where $\langle a^2 \rangle$ is the mean square droplet radius.

4. A PHYSICAL MODEL FOR COMMINUTION

The central issue is clear from equation (9): What are the processes - and thus the liquid characteristics - that determine the mean square droplet size? We assume that the mechanism of droplet formation is mainly a mechanical (as opposed to a thermal) one. At any instant even an equilibrium liquid exhibits local deviations from homogeneity and isotropy. One characterization of the deviations from homogeneity is the distribution of fluctuations in the density. From classical statistical mechanics the probability of occurrence of a density fluctuation in the range $\Delta\rho$ to $\Delta\rho + d\rho$ is

$$P(\Delta\rho)d\rho = (2\pi \langle \Delta\rho^2 \rangle)^{-1/2} \exp[-\Delta\rho^2/2\langle \Delta\rho^2 \rangle] d\rho, \quad (10)$$

where $\langle \Delta\rho^2 \rangle$ is the mean square density fluctuation given by

$$\langle \Delta\rho^2 \rangle = \rho^2 (kT/V)/K, \quad (11)$$

where T and ρ are the temperature and average density of the system, V is the volume of the region under consideration, k is Boltzmann's constant, and K is the equilibrium bulk modulus of the material.

We suggest that under the influence of the large explosively generated stresses, these local inhomogeneities will behave as structural flaws in the material: shear stresses tend to

elongate the inhomogeneities by "organizing" the liquid structure* while the tensile stresses cause the flaws to propagate at the stress intensification points. The situation is depicted pictorially in figure 1. However, in a liquid, even at the elevated pressures produced by the explosive shock, one expects that the rate at which the flaws heal and the rate at which they propagate via growth at their tips should be comparable; consequently, one is not dealing with a classical brittle fracture situation, but rather one involving relatively little growth. Thus the maximum flaw dimension should be comparable with the size of the particles that result from the explosive comminution.

It is the processes described in this last paragraph that will depend sensitively on the nonlinear viscoelastic response characteristics of the liquid system. Because the large stresses to which the material is subjected are "switched on" essentially instantaneously, the nature of the behavior will be governed in large measure by the characteristic time scales of the shear and structural responses of the liquid, i.e., the shear and structural relaxation times. The specific picture that we have described above is an oversimplified one in which we have assumed that the shear relaxation time is negligibly small in comparison with the structural relaxation time. Only in this limiting situation is one able to portray the flaw development and liquid fracture processes without reference to the specific viscoelastic and strength parameters that describe the material. Generally speaking these extreme conditions do not obtain; the shear relaxation time, while smaller than the structural time, is of the same order of magnitude. Consequently, the sequential nature of the mechanisms that operate in comminution that was assumed above — the development of large shear strains, followed by structural reorganization (flaw development), followed by liquid fracture from tensile stresses — is not nearly so precisely defineable. The various mechanisms do not proceed strictly serially, but rather couple in a complicated interactive and, perhaps, competitive fashion. Depending upon the relative time scales and specific forms of the various response mechanisms, this coupling can either reinforce the liquid comminution process (leading to smaller particle sizes) or interfere with it (resulting in larger particle sizes). Nevertheless, the elementary picture that we are examining is a useful one for it provides a general framework in which to analyze and compare the behavior of different liquids acted on by explosive stresses, as well as highlighting the crucial liquid properties that govern (at least in lowest order approximation) the cloud dispersal characteristics.

In order to estimate the droplet size, we can employ the following sort of elementary notions. We consider that in order to generate droplets of characteristic dimension = a , a region of the liquid of volume $V \approx a^3$ must contain a flaw whose volume exceeds some critical volume V_c . The action of the explosive shear stresses is to elongate and shape the flaw [into roughly a "pillow" shape (see figure 2)] so that it can be described by dimensions a , b , and c ($a > b > c$). The minimum flaw volume $V_c = abc$, that will lead to the production of droplets with dimensions on the order of " a " will result if one has a local density fluctuation

$$\Delta\rho >= \rho V_c/V \equiv \Delta\rho_c \quad (12)$$

in the volume V . The liquid will comminute into particles of this size only if a fluctuation of such magnitude occurs with significant probability. The condition for this to obtain is

$$\Delta\rho_c \approx \langle \Delta\rho^2 \rangle^{1/2}; \quad (13)$$

* Heyes, D. M., Kim, J. J., Montrose, C. J. and Litovitz, T. A. Time-Dependent Non-Linear Shear Stress Effects in Simple Liquids: A Molecular Dynamics Study. *J. Chem. Phys.* 73, 3987 (1980).

elongate the inhomogeneities by "organizing" the liquid structure* while the tensile stresses cause the flaws to propagate at the stress intensification points. The situation is depicted pictorially in figure 1. However, in a liquid, even at the elevated pressures produced by the explosive shock, one expects that the rate at which the flaws heal and the rate at which they propagate via growth at their tips should be comparable; consequently, one is not dealing with a classical brittle fracture situation, but rather one involving relatively little growth. Thus the maximum flaw dimension should be comparable with the size of the particles that result from the explosive comminution.

It is the processes described in this last paragraph that will depend sensitively on the nonlinear viscoelastic response characteristics of the liquid system. Because the large stresses to which the material is subjected are "switched on" essentially instantaneously, the nature of the behavior will be governed in large measure by the characteristic time scales of the shear and structural responses of the liquid, i.e., the shear and structural relaxation times. The specific picture that we have described above is an oversimplified one in which we have assumed that the shear relaxation time is negligibly small in comparison with the structural relaxation time. Only in this limiting situation is one able to portray the flaw development and liquid fracture processes without reference to the specific viscoelastic and strength parameters that describe the material. Generally speaking these extreme conditions do not obtain; the shear relaxation time, while smaller than the structural time, is of the same order of magnitude. Consequently, the sequential nature of the mechanisms that operate in comminution that was assumed above — the development of large shear strains, followed by structural reorganization (flaw development), followed by liquid fracture from tensile stresses — is not nearly so precisely defineable. The various mechanisms do not proceed strictly serially, but rather couple in a complicated interactive and, perhaps, competitive fashion. Depending upon the relative time scales and specific forms of the various response mechanisms, this coupling can either reinforce the liquid comminution process (leading to smaller particle sizes) or interfere with it (resulting in larger particle sizes). Nevertheless, the elementary picture that we are examining is a useful one for it provides a general framework in which to analyze and compare the behavior of different liquids acted on by explosive stresses, as well as highlighting the crucial liquid properties that govern (at least in lowest order approximation) the cloud dispersal characteristics.

In order to estimate the droplet size, we can employ the following sort of elementary notions. We consider that in order to generate droplets of characteristic dimension = a , a region of the liquid of volume $V \approx a^3$ must contain a flaw whose volume exceeds some critical volume V_c . The action of the explosive shear stresses is to elongate and shape the flaw [into roughly a "pillow" shape (see figure 2)] so that it can be described by dimensions a , b , and c ($a > b > c$). The minimum flaw volume $V_c = abc$, that will lead to the production of droplets with dimensions on the order of " a " will result if one has a local density fluctuation

$$\Delta\rho >= \rho V_c/V \equiv \Delta\rho_c \quad (12)$$

in the volume V . The liquid will comminute into particles of this size only if a fluctuation of such magnitude occurs with significant probability. The condition for this to obtain is

$$\Delta\rho_c \approx \langle \Delta\rho^2 \rangle^{1/2}; \quad (13)$$

* Heyes, D. M., Kim, J. J., Montrose, C. J. and Litovitz, T. A. Time-Dependent Non-Linear Shear Stress Effects in Simple Liquids: A Molecular Dynamics Study. *J. Chem. Phys.* 73, 3987 (1980).

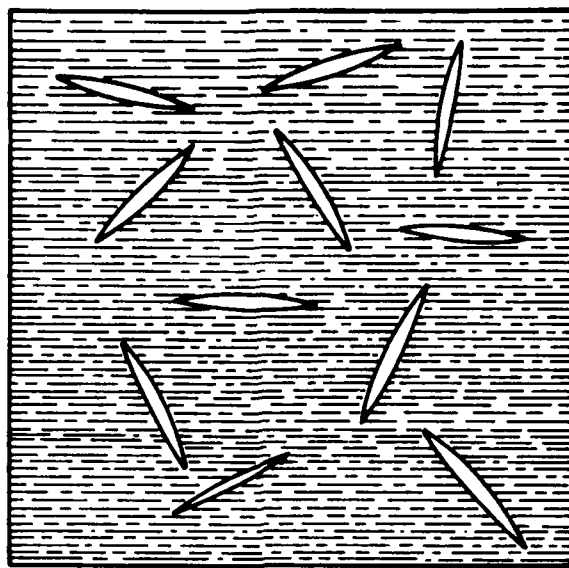


Figure 1.A. A Schematic Representation of Liquid Flaws Elongated under the Action of Large Shear Stresses

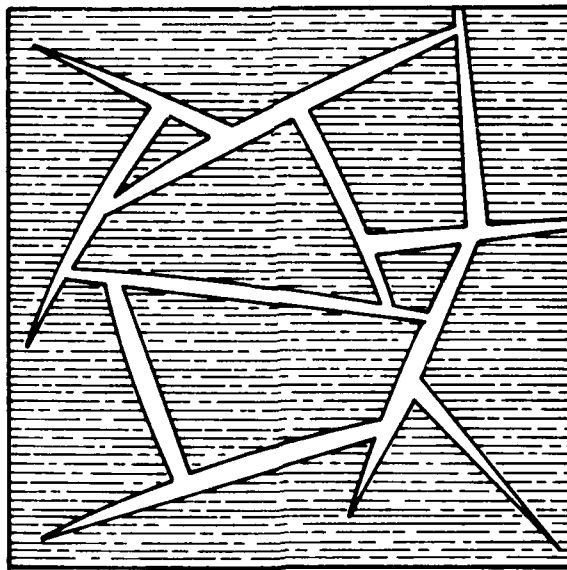


Figure 1.B. Liquid Flaws That Have Grown and Intersected to Form Comminution Droplets under the Action of Tensile Stresses.

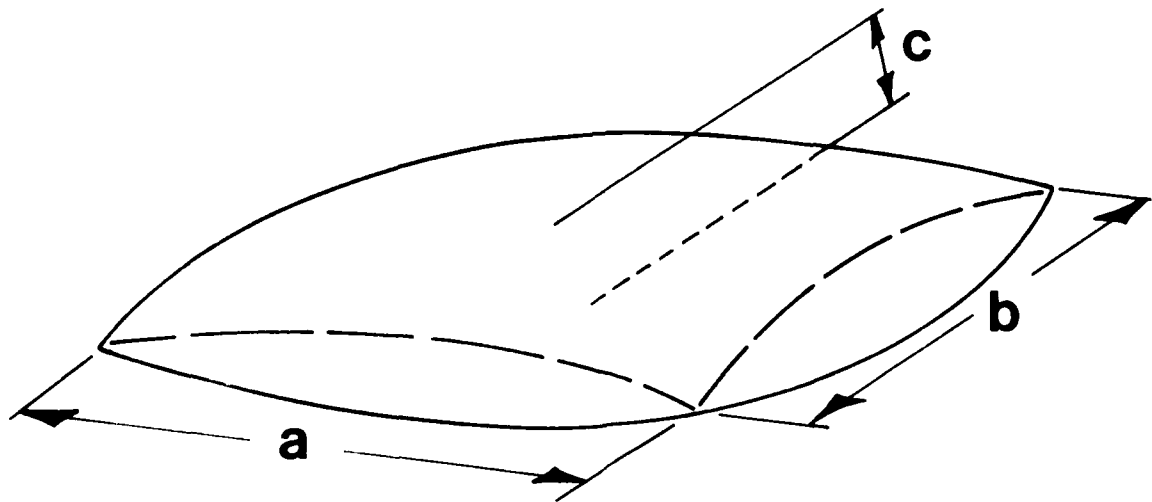


Figure 2. A Flaw of Critical Size: **a** is the Largest Dimension, **c** the Smallest.

that is, the critical density fluctuation must be comparable with the RMS density fluctuation. Substituting equations (11) and (12) in equation (13) and using $V \approx a^3$ and $V = abc$ leads to an approximate expression for the value of a :

$$a \approx (bc)^2 K/kT. \quad (14)$$

Recalling equation (9), this leads to an equation for the mean height of the droplets:

$$\langle z \rangle \approx (2/9\eta) v_0 \rho (bc)^4 (K/kT)^2. \quad (15)$$

In order that the flaws do not heal themselves too rapidly, it is essential that the smallest flaw dimension c be at least on the order of a molecular separation distance; with this in mind we have

$$c \propto \rho^{-1/3} \quad (16)$$

and recalling that $v_0 \propto \rho^{-1/2}$, we may collect together all the density-dependent quantities on the right hand side of equation (15). The resulting expression takes the form

$$\langle z \rangle \propto \rho^{-5/6} K^2. \quad (17)$$

5. COMPARISON WITH EXPERIMENT

Equation (17) is in a form that can be compared with experimental results. The comparison is shown in figure 3 for six liquids at 20°C. Many of the data for this figure were taken from the work of Gerber and Stuempfle* and are presented in the table which will follow. As is apparent there is fairly good agreement between these data and the prediction of equation (17) (the slope of the line shown in figure 3 is $65.5 \text{ g}^{5/6} \text{ cm}^{-3/2} \text{ GPa}^{-2}$). This offers fairly strong support for the essential correctness of the view of the comminution mechanism that was described above. It is also clear that the modifications of this overly simplified view that are required if one correctly treats the dynamical aspects of the liquid response are not understood in any kind of quantitative fashion. Some of the molecular dynamics results (presented in the appendix) give a fair indication of the type of phenomena that must be considered — especially in regard to liquid structural changes occasioned by large shear stress — but efforts to apply these results quantitatively to comminution are at this point premature.

Of the six liquids which were considered above, except for carbon tetrachloride, comminution data have also been obtained at 130°C. The variation that one would expect from our model is given by equation (15); the major effect appears to be the factor $(1/kT)^2$. On the basis of this one would expect the ratio of the mean height at 20°C to that at 130°C would be about $(403/293)^2 \approx 1.9$. The experimentally determined ratios for the liquids that we have considered fall into the range of about 1.0 to 1.5.

*Gerber, B. V., and Stuempfle, A. D., op. cit.

that is, the critical density fluctuation must be comparable with the RMS density fluctuation. Substituting equations (11) and (12) in equation (13) and using $V \approx a^3$ and $V = abc$ leads to an approximate expression for the value of a :

$$a \approx (bc)^2 K/kT. \quad (14)$$

Recalling equation (9), this leads to an equation for the mean height of the droplets:

$$\langle z \rangle \approx (2/9\eta) v_0 \rho (bc)^4 (K/kT)^2. \quad (15)$$

In order that the flaws do not heal themselves too rapidly, it is essential that the smallest flaw dimension c be at least on the order of a molecular separation distance; with this in mind we have

$$c \propto \rho^{-1/3} \quad (16)$$

and recalling that $v_0 \propto \rho^{-1/2}$, we may collect together all the density-dependent quantities on the right hand side of equation (15). The resulting expression takes the form

$$\langle z \rangle \propto \rho^{-5/6} K^2. \quad (17)$$

5. COMPARISON WITH EXPERIMENT

Equation (17) is in a form that can be compared with experimental results. The comparison is shown in figure 3 for six liquids at 20°C. Many of the data for this figure were taken from the work of Gerber and Stuempfle* and are presented in the table which will follow. As is apparent there is fairly good agreement between these data and the prediction of equation (17) (the slope of the line shown in figure 3 is $65.5 \text{ g}^{5/6} \text{ cm}^{-3/2} \text{ GPa}^{-2}$). This offers fairly strong support for the essential correctness of the view of the comminution mechanism that was described above. It is also clear that the modifications of this overly simplified view that are required if one correctly treats the dynamical aspects of the liquid response are not understood in any kind of quantitative fashion. Some of the molecular dynamics results (presented in the appendix) give a fair indication of the type of phenomena that must be considered — especially in regard to liquid structural changes occasioned by large shear stress — but efforts to apply these results quantitatively to comminution are at this point premature.

Of the six liquids which were considered above, except for carbon tetrachloride, comminution data have also been obtained at 130°C. The variation that one would expect from our model is given by equation (15); the major effect appears to be the factor $(1/kT)^2$. On the basis of this one would expect the ratio of the mean height at 20°C to that at 130°C would be about $(403/293)^2 \approx 1.9$. The experimentally determined ratios for the liquids that we have considered fall into the range of about 1.0 to 1.5.

*Gerber, B. V., and Stuempfle, A. D., op. cit.

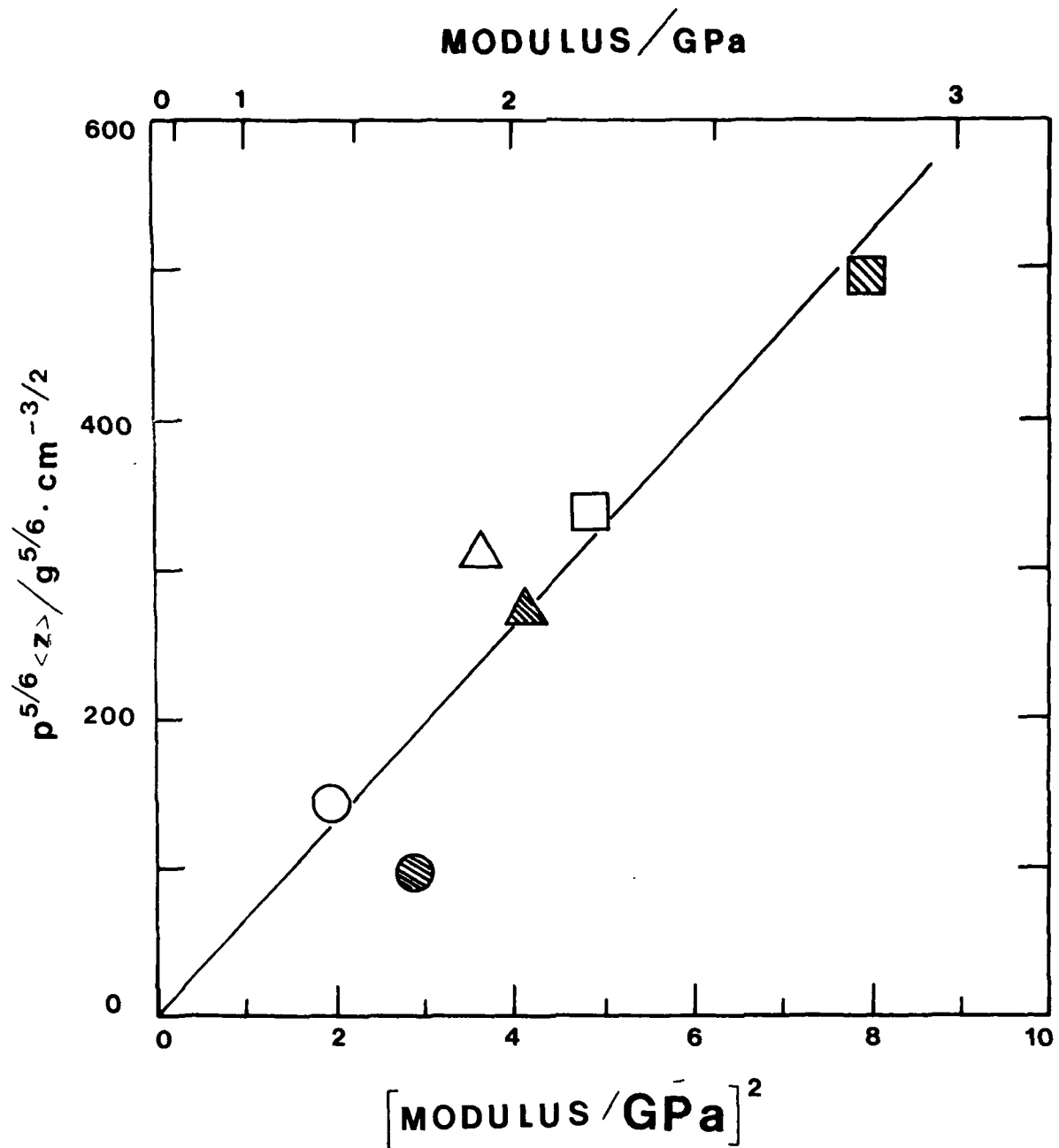


Figure 3. The Mean Height to Which the Droplets Rise Multiplied by Density to the 5/6 Power Plotted Versus the Square of the Bulk Modulus. The Solid Line Is Drawn According to Equation (17). The data shown are for the six liquids listed in table 1 (where the various symbols are identified) at a temperature of 20°C.

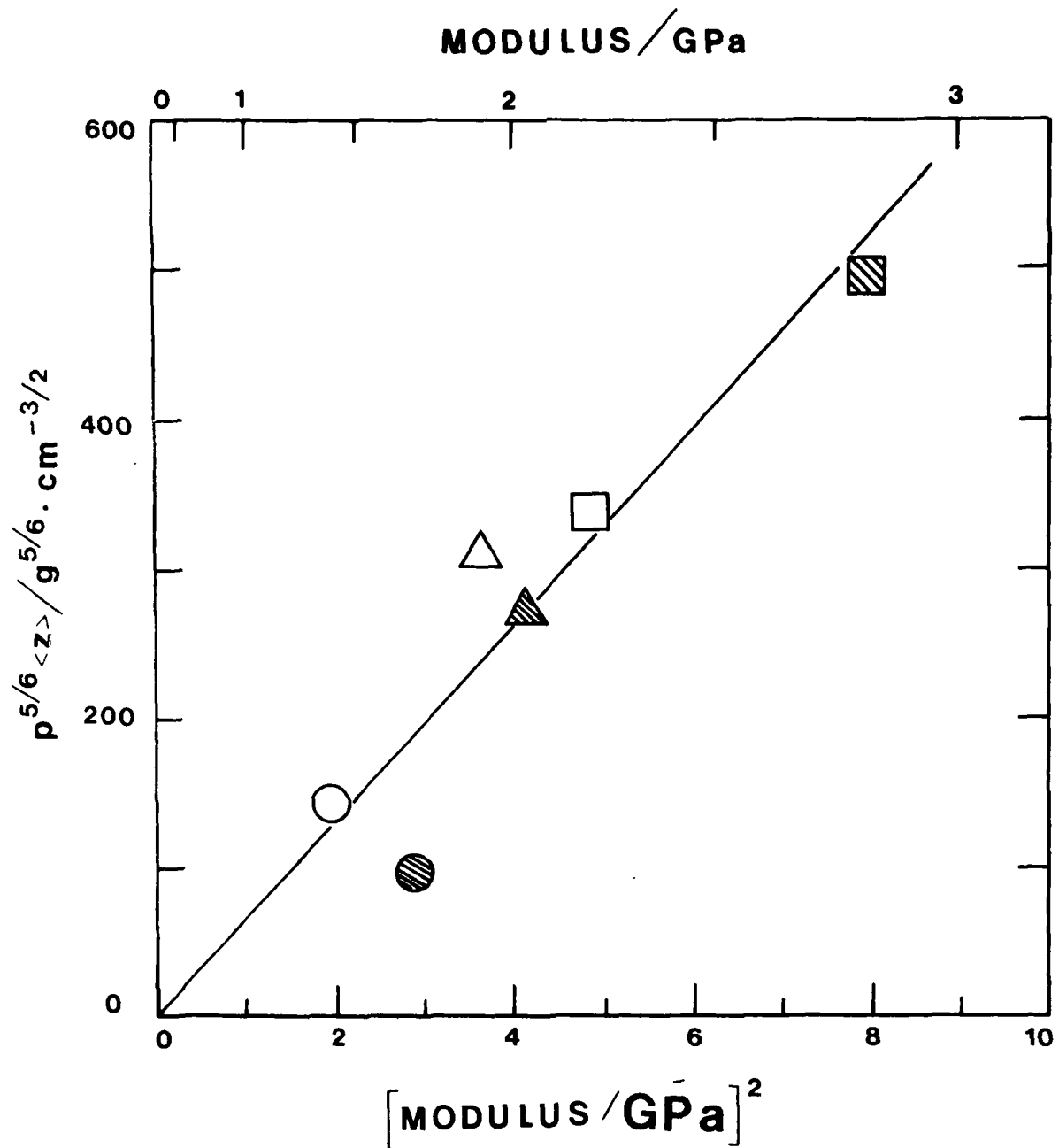


Figure 3. The Mean Height to Which the Droplets Rise Multiplied by Density to the 5/6 Power Plotted Versus the Square of the Bulk Modulus. The Solid Line Is Drawn According to Equation (17). The data shown are for the six liquids listed in table 1 (where the various symbols are identified) at a temperature of 20°C.

Table. Data Used in Constructing Figure 3. All Data Are Given for a Temperature of 20°C.

Liquid	Density	$\langle z \rangle$	Modulus
Tetrachloroethylene (○)	(g/cm ³) 1.62	(cm) 64	(GPa) ^a 1.8
Carbon tetrachloride (●)	1/59	96	1.39
2,2-dichloroethanol (Δ)	1.40	232	1.91
1,2,3-trichloropropane (▲)	1.61	182	2.03
Water (□)	1.00	336	2.24
Tetrabromoethane (■)	2.91	201	2.81

$$(a) 1\text{GPa} = 10^9\text{N/m}^2 = 10^{10}\text{dyne/cm}^2 = 145.5 \text{ kpsi}$$

This cannot be accounted for by considering the change with temperature of the density and the modulus. It probably reflects the increasingly important role of the viscoelastic responses, for which the relaxation times will be significantly shorter at the higher temperature.

6. THE EFFECT OF POLYMERIC ADDITIVES

Gerber and Stuempfle* also report measurements at 20°C on two samples of tetrachloroethylene to one of which was added 1% polvisobutylene (PIB), while the other contained 1% polystyrene (PS). In the former case $\langle z \rangle$ was increased by nearly a factor of four while in the latter case the increase was less than 50%. Phrased another way, the effect of PIB is nearly to double the average droplet radius, whereas PS produces only about a 20% increase in droplet size. The model of comminution that we have considered would lead one to expect an increase in droplet size on the order of 10% or less. Clearly some other mechanism is operative in determining the particle size. We suggest that the effect of the polymeric molecules is to act as agents that terminate the flaws by inhibiting their growth under the applied stresses. The PIB molecules, which were of substantially greater average chain length, are much more effective in this regard than the (relatively shorter) PS molecules, and thus lead to the formation of rather large droplets.

7. SUMMARY AND CONCLUSIONS

In this report we have presented a physical model of the explosive comminution process in liquids. The key feature of the model involves the development of flaws in the liquid under the action of large explosively generated stresses. It is at these flaws that the material fails via a process that we have termed "liquid fracture." Guided by previous molecular dynamics (MD) studies that we have carried out on the nonlinear response character of liquids (a partial summary of these is given in the Appendix), we have proposed a highly simplified view of this

*Gerber, B. V., and Stuempfle, A. D., op. cit.

Table. Data Used in Constructing Figure 3. All Data Are Given for a Temperature of 20°C.

Liquid	Density	$\langle z \rangle$	Modulus
Tetrachloroethylene (○)	(g/cm ³) 1.62	(cm) 64	(GPa) ^a 1.8
Carbon tetrachloride (●)	1/59	96	1.39
2,2-dichloroethanol (Δ)	1.40	232	1.91
1,2,3-trichloropropane (▲)	1.61	182	2.03
Water (□)	1.00	336	2.24
Tetrabromoethane (■)	2.91	201	2.81

$$(a) 1\text{GPa} = 10^9\text{N/m}^2 = 10^{10}\text{dyne/cm}^2 = 145.5 \text{ kpsi}$$

This cannot be accounted for by considering the change with temperature of the density and the modulus. It probably reflects the increasingly important role of the viscoelastic responses, for which the relaxation times will be significantly shorter at the higher temperature.

6. THE EFFECT OF POLYMERIC ADDITIVES

Gerber and Stuempfle* also report measurements at 20°C on two samples of tetrachloroethylene to one of which was added 1% polvisobutylene (PIB), while the other contained 1% polystyrene (PS). In the former case $\langle z \rangle$ was increased by nearly a factor of four while in the latter case the increase was less than 50%. Phrased another way, the effect of PIB is nearly to double the average droplet radius, whereas PS produces only about a 20% increase in droplet size. The model of comminution that we have considered would lead one to expect an increase in droplet size on the order of 10% or less. Clearly some other mechanism is operative in determining the particle size. We suggest that the effect of the polymeric molecules is to act as agents that terminate the flaws by inhibiting their growth under the applied stresses. The PIB molecules, which were of substantially greater average chain length, are much more effective in this regard than the (relatively shorter) PS molecules, and thus lead to the formation of rather large droplets.

7. SUMMARY AND CONCLUSIONS

In this report we have presented a physical model of the explosive comminution process in liquids. The key feature of the model involves the development of flaws in the liquid under the action of large explosively generated stresses. It is at these flaws that the material fails via a process that we have termed "liquid fracture." Guided by previous molecular dynamics (MD) studies that we have carried out on the nonlinear response character of liquids (a partial summary of these is given in the Appendix), we have proposed a highly simplified view of this

*Gerber, B. V., and Stuempfle, A. D., op. cit.

process. Even this simplified picture is relatively successful in yielding semiquantitative agreement with experimental data.

In order to develop a truly quantitative picture, it is our belief that the dynamical aspects of the liquid failure mechanisms must be more fully understood. A thoroughgoing molecular dynamics investigation of the time-dependent structural response of liquids to high-amplitude shear and tensile stresses would prove most useful in elucidating the essential features of these nonlinear viscoelastic dynamics that operate in explosive comminution. We are at present examining the possibilities of initiating such an effort.

process. Even this simplified picture is relatively successful in yielding semiquantitative agreement with experimental data.

In order to develop a truly quantitative picture, it is our belief that the dynamical aspects of the liquid failure mechanisms must be more fully understood. A thoroughgoing molecular dynamics investigation of the time-dependent structural response of liquids to high-amplitude shear and tensile stresses would prove most useful in elucidating the essential features of these nonlinear viscoelastic dynamics that operate in explosive comminution. We are at present examining the possibilities of initiating such an effort.

APPENDIX

MOLECULAR DYNAMICS

Not only in the process of comminution but also in a rather wide variety of technological applications, for example elastohydrodynamic lubrication, shock loading, solid propellant failures, etc., liquids and amorphous solids are subjected to extremely large shearing forces. Because the microscopic mechanisms of importance are not well understood, solutions to problems involving nonlinear behavior are quite limited.

For example in order to predict shear failure (or tearing) of a liquid under the forces of an explosion or shock wave, one must be able to compute the time evolution of the stress in a fluid element when it encounters a simultaneously applied time varying shear rate and a time varying pressure. The response of the system under these conditions can, for low shearing rates, be parameterized in terms of the shear viscosity, η , a shear rigidity modulus, G_∞ , and a distribution of relaxation times. At the rather large shearing rates generally encountered, this relatively simple description must be modified to incorporate the nonlinear character of the dynamical stress response. Some authors* suppose that this can be done by appending the idea of a limiting shear stress to the low amplitude, i.e., linear, shear response. In order to test this hypothesis and, more generally, to provide a framework on which to base analytical representations of nonlinear viscoelastic behavior, we have used Molecular Dynamics (MD) to investigate a model liquid system under conditions approximating those found in at high shear rates. Even though the model system is particularly simple, we have been able to reproduce the major features of shear response of real liquids. Because an MD experiment provides one with a complete microscopic record of the system's evolution in time, one can perform "experiments" and "measure" aspects of its behavior that are not accessible in conventional experiments, but which provide useful insights into the origin of the properties of liquids under extreme stress conditions.

The MD calculation procedure observes a portion of liquid as it is sheared. Although a simultaneously applied time dependent pressure and shear rate would more closely represent the conditions of a liquid undergoing explosive comminution, we have confined our attention up to now to considering the response of a model fluid to a time varying shear rate at a series of densities (pressures).

THE MODEL

MD is a computer simulation technique for probing the microscopic behavior of a system that allows one to account for the many-body nature of the molecular interactions. It involves following some representative number of molecules, N , by solving the classical equations of motion on a high speed computer to obtain their trajectories in time steps of typically 0.01 ps. Since only rather a limited number of molecules is treated (generally less than a thousand), the molecules are confined in a cubic box which is surrounded by images of itself to avoid severe boundary effects. In the studies described below the artificialities introduced by this procedure are rather insignificant. From the results of an MD "experiment" — essentially a record of the system's path through phase space — one can determine any measurable property of the system, as well as many that are experimentally inaccessible.

*Bair, S., and Winer, W. O. A Rheological Model for Elastohydrodynamic Contacts Based on Primary Laboratory Data, ASME J. Lub. Tech., 101, 258 (1979).

APPENDIX

MOLECULAR DYNAMICS

Not only in the process of comminution but also in a rather wide variety of technological applications, for example elastohydrodynamic lubrication, shock loading, solid propellant failures, etc., liquids and amorphous solids are subjected to extremely large shearing forces. Because the microscopic mechanisms of importance are not well understood, solutions to problems involving nonlinear behavior are quite limited.

For example in order to predict shear failure (or tearing) of a liquid under the forces of an explosion or shock wave, one must be able to compute the time evolution of the stress in a fluid element when it encounters a simultaneously applied time varying shear rate and a time varying pressure. The response of the system under these conditions can, for low shearing rates, be parameterized in terms of the shear viscosity, η , a shear rigidity modulus, G_∞ , and a distribution of relaxation times. At the rather large shearing rates generally encountered, this relatively simple description must be modified to incorporate the nonlinear character of the dynamical stress response. Some authors* suppose that this can be done by appending the idea of a limiting shear stress to the low amplitude, i.e., linear, shear response. In order to test this hypothesis and, more generally, to provide a framework on which to base analytical representations of nonlinear viscoelastic behavior, we have used Molecular Dynamics (MD) to investigate a model liquid system under conditions approximating those found in at high shear rates. Even though the model system is particularly simple, we have been able to reproduce the major features of shear response of real liquids. Because an MD experiment provides one with a complete microscopic record of the system's evolution in time, one can perform "experiments" and "measure" aspects of its behavior that are not accessible in conventional experiments, but which provide useful insights into the origin of the properties of liquids under extreme stress conditions.

The MD calculation procedure observes a portion of liquid as it is sheared. Although a simultaneously applied time dependent pressure and shear rate would more closely represent the conditions of a liquid undergoing explosive comminution, we have confined our attention up to now to considering the response of a model fluid to a time varying shear rate at a series of densities (pressures).

THE MODEL

MD is a computer simulation technique for probing the microscopic behavior of a system that allows one to account for the many-body nature of the molecular interactions. It involves following some representative number of molecules, N , by solving the classical equations of motion on a high speed computer to obtain their trajectories in time steps of typically 0.01 ps. Since only rather a limited number of molecules is treated (generally less than a thousand), the molecules are confined in a cubic box which is surrounded by images of itself to avoid severe boundary effects. In the studies described below the artificialities introduced by this procedure are rather insignificant. From the results of an MD "experiment" — essentially a record of the system's path through phase space — one can determine any measurable property of the system, as well as many that are experimentally inaccessible.

*Bair, S., and Winer, W. O. A Rheological Model for Elastohydrodynamic Contacts Based on Primary Laboratory Data, ASME J. Lub. Tech., 101, 258 (1979).

The model system we consider here is an assembly of 108 Lennard-Jones (LJ) particles; these molecules interact through pairwise additive forces described by the LJ 6-12 potential,

$$\Phi(r) = -4u \left[(a/r)^6 - (a/r)^{12} \right], \quad (1)$$

where r is the separation of an interacting pair, and u and a are constants with dimensions of energy and distance, respectively. All the computed quantities are in so-called LJ reduced units which are given in terms of u , a , and m , the mass of an individual particle. Although no real liquid can be characterized by a potential of the LJ form (only the noble gas fluids Ar, Kr, etc., are quantitatively represented in this way) their structural and dynamical behavior can be expected to be (and we have found actually are) qualitatively similar to that of the model fluid. As a result one can expect that the microscopic insights derived from MD experiments will serve as useful guidelines for understanding and modeling the behavior of real liquids and perhaps for the "molecular engineering" of improved comminution properties of liquids. For the purpose of comparison with experiment frequent conversion from reduced to "real" units will be made, using the parameters for Ar which are given in table A-1.

Table A-1. A Summary of the Reduced Units in Terms of Which All Quantities Are Given.
Boltzmann's constant is denoted by k_B .

Quantity	Reduced Unit	SI Unit for Ar
distance	a	0.3405 nm
mass	m	6.64×10^{-26} kg
energy	u	1.65×10^{-21} J
time	$a(m/u)^{1/2}$	2.16 ps
density	a^{-3}	42.1 kg mol/m ³
temperature	u/k_B	119.8 K
pressure, stress	u/a^3	41.8 MPa
modulus	u/a^3	41.8 MPa
viscosity	$(mu)^{1/2}/a^2$	9.03×10^{-5} Pa s
thermal conductivity	$k_B (m/u)^{-1/2} a^{-2}$	1.88×10^{-2} J m ⁻¹ K ⁻¹ s ⁻¹

Two methods of shearing the box of molecules can be used. The results of each method agree within statistical error; however, each method is well suited to examine a particular aspect of the investigated phenomenon.

The first method attempts to mimic a situation in which the fluid forms a thin film.

The model system we consider here is an assembly of 108 Lennard-Jones (LJ) particles; these molecules interact through pairwise additive forces described by the LJ 6-12 potential,

$$\Phi(r) = -4u \left[(a/r)^6 - (a/r)^{12} \right], \quad (1)$$

where r is the separation of an interacting pair, and u and a are constants with dimensions of energy and distance, respectively. All the computed quantities are in so-called LJ reduced units which are given in terms of u , a , and m , the mass of an individual particle. Although no real liquid can be characterized by a potential of the LJ form (only the noble gas fluids Ar, Kr, etc., are quantitatively represented in this way) their structural and dynamical behavior can be expected to be (and we have found actually are) qualitatively similar to that of the model fluid. As a result one can expect that the microscopic insights derived from MD experiments will serve as useful guidelines for understanding and modeling the behavior of real liquids and perhaps for the "molecular engineering" of improved comminution properties of liquids. For the purpose of comparison with experiment frequent conversion from reduced to "real" units will be made, using the parameters for Ar which are given in table A-1.

Table A-1. A Summary of the Reduced Units in Terms of Which All Quantities Are Given.
Boltzmann's constant is denoted by k_B .

Quantity	Reduced Unit	SI Unit for Ar
distance	a	0.3405 nm
mass	m	6.64×10^{-26} kg
energy	u	1.65×10^{-21} J
time	$a(m/u)^{1/2}$	2.16 ps
density	a^{-3}	42.1 kg mol/m ³
temperature	u/k_B	119.8 K
pressure, stress	u/a^3	41.8 MPa
modulus	u/a^3	41.8 MPa
viscosity	$(mu)^{1/2}/a^2$	9.03×10^{-5} Pa s
thermal conductivity	$k_B (m/u)^{-1/2} a^{-2}$	1.88×10^{-2} J m ⁻¹ K ⁻¹ s ⁻¹

Two methods of shearing the box of molecules can be used. The results of each method agree within statistical error; however, each method is well suited to examine a particular aspect of the investigated phenomenon.

The first method attempts to mimic a situation in which the fluid forms a thin film. This thin film is achieved in the model system by employing periodicity in the x and y directions only; the external shear forces are applied by two fluid layers translating with the desired wall velocities, U_1 and U_2 . Molecules from the three regions (i.e., the two wall regions and the liquid itself) are not allowed to mix and are kept from doing so by reflection boundary conditions in the z direction. The fluid walls (FW) are maintained at a preset temperature by adjusting their velocities at each time step of the integration scheme.

The second method is a modification of the Homogeneous Shear technique* (MHS), which is better suited to study the viscoelastic behavior of the fluid because it employs periodicity in all directions so that a bulk material is sheared. It also enables a desired strain rate to be instantaneously achieved throughout the liquid. The molecular trajectories are disturbed from those governed by equilibrium fluctuations by imposing a shear strain rate, $\dot{\epsilon}$, on the system. This is accomplished by displacing (after each time step, Δt) the x-coordinate of the i'th molecule in the MD cell by an amount $\delta x_i = \dot{\epsilon} z_i \Delta t$, where z_i is the z coordinate of particle i and Δt is the length of the time step, for as long as the shearing is required. The results of this technique, in particular those relating to viscoelasticity (derived using a time dependent strain rate), complement those of the FW method.

We have used non-equilibrium MD experiments to investigate the linear and nonlinear shear response of the LJ system under a variety of thermodynamic conditions. The temperature, T , and number density, ρ , initially studied were close to the normal freezing temperature, T_f , of the LJ liquid, that is $0.722 k_B T/u$ and $0.8442 N_A^3/V$, respectively. Densifications of 10%, 20%, and 50% relative to the starting density were achieved by suddenly (within one time step) compressing the system at constant temperature. The densifications were achieved so rapidly that the systems were kinetically prevented from crystallizing.

MD "MEASUREMENT" OF SHEAR VISCOSITY OF HIGH STRAIN RATES

We first consider the dependence of shear viscosity on shear rate in the nonlinear region. In the Homogeneous Shear method a uniform x velocity profile was set up instantaneously whereas a period of several time units was required for the fluid walls to drive the central region into this state. An x velocity gradient was achieved by maintaining the upper and lower walls at velocities of U and $-U$, respectively. An example of a $v_x(z)$ so derived is shown in figure A-1. The value of $\dot{\epsilon}$ corresponds to an extremely large shear rate — on the order of $10^{10} s^{-1}$, depending somewhat upon the particular values of u , a , and m that are chosen. Such large values of $\dot{\epsilon}$ were chosen since it is desirable to explore the system's behavior at shear rates on the order of the reciprocal of the viscoelastic relaxation times. For the LJ fluids these are approximately unity (about $10^{-12} s$). The shear stress needed to define a shear viscosity is readily derived from the velocities and positions of the molecules. The $\alpha\beta$ component of the stress tensor is defined below,

$$\sigma_{\alpha\beta} = -(1/V) \left[\sum_{i=1}^N m v_i^\alpha v_i^\beta - \frac{1}{2} \sum_i \sum_j (\alpha_{ij} \beta_{ij} / r_{ij}) \frac{\partial \phi}{\partial r_{ij}} \right] \quad (2)$$

where V is the volume of the MD cell, v_i^α is the α velocity component of molecule i relative to the average velocity and α_{ij} is the α component of the separation between molecules i and j. The subscripts for the shear stress component, σ_{xz} , are dropped in further discussion.

At low shear rates plots of shear stress versus strain rate, $\dot{\epsilon}$, are linear; however, at high stress levels ($\sim G_\infty / 100$) the shear stress increases less rapidly than $\dot{\epsilon}$. In other words the shear viscosity ($= \sigma/\dot{\epsilon}$) decreases from the equilibrium (or zero shear rate) value of η_0 with increasing shear rate. The MHS method was used to obtain η versus $\dot{\epsilon}$ for a variety of densities. The forms of η/η_0 versus stress in figure A-2 resemble closely those obtained from twin-disk experiments for the fluids 5P4E, and the lubricants L63/1271 and Oxilube 85/140 after making the appropriate conversions to real units. The ratio η/η_0 descends markedly from unity in the region ~ 50 MPa. The decrease in η with $\dot{\epsilon}$ is not due to thermal heating because the calculations were conducted isothermally.

*Heyes, D. M. et al., op. cit.

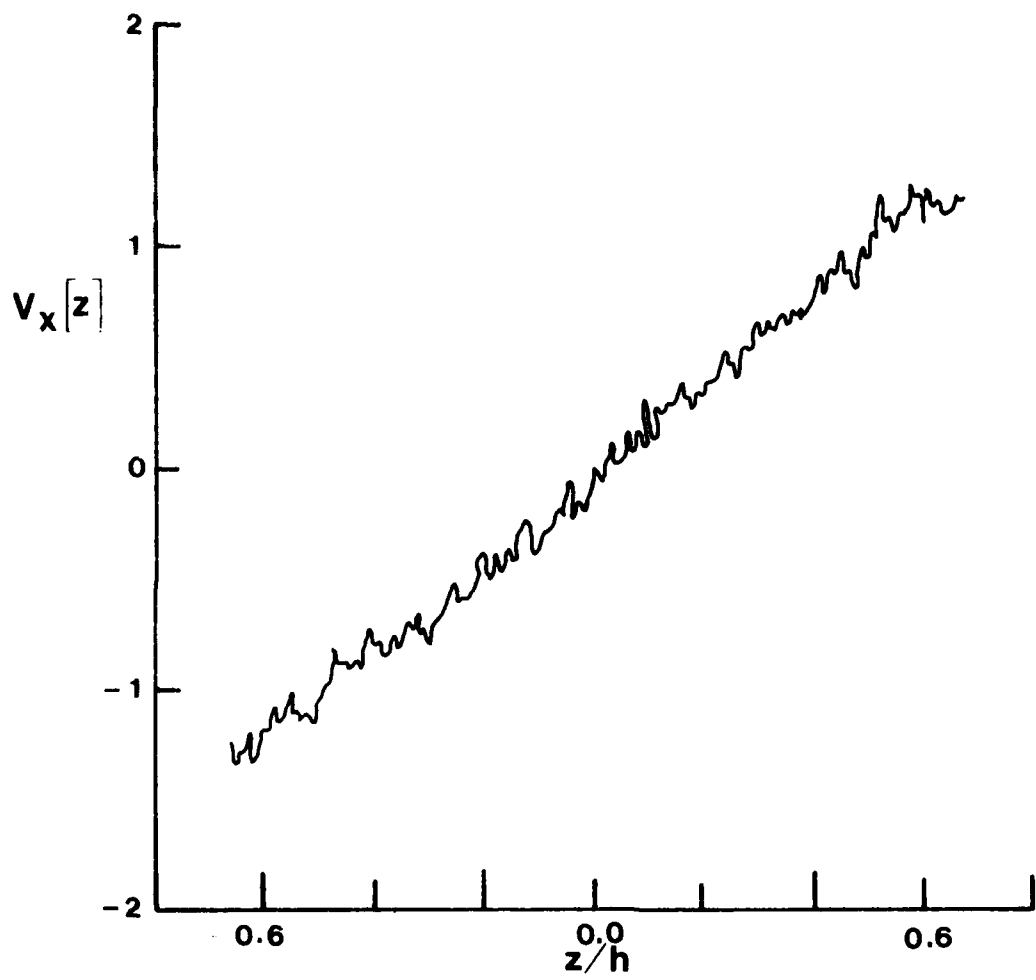


Figure A-1. The z Dependence of the Average x Velocity for the $\rho = 0.8442$ and $i = 0.3373$ State Using the FW Model. The z coordinate system is measured from the center of the film.

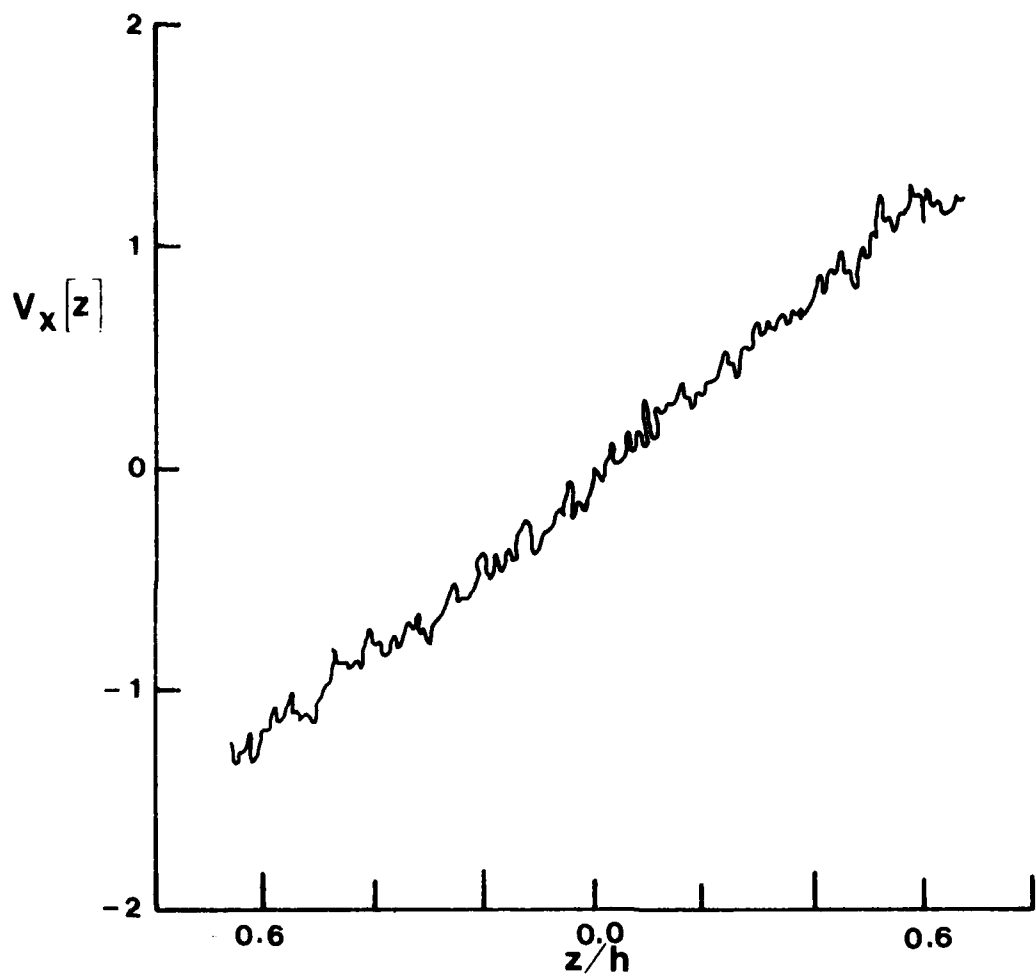


Figure A-1. The z Dependence of the Average x Velocity for the $\rho = 0.8442$ and $i = 0.3373$ State Using the FW Model. The z coordinate system is measured from the center of the film.

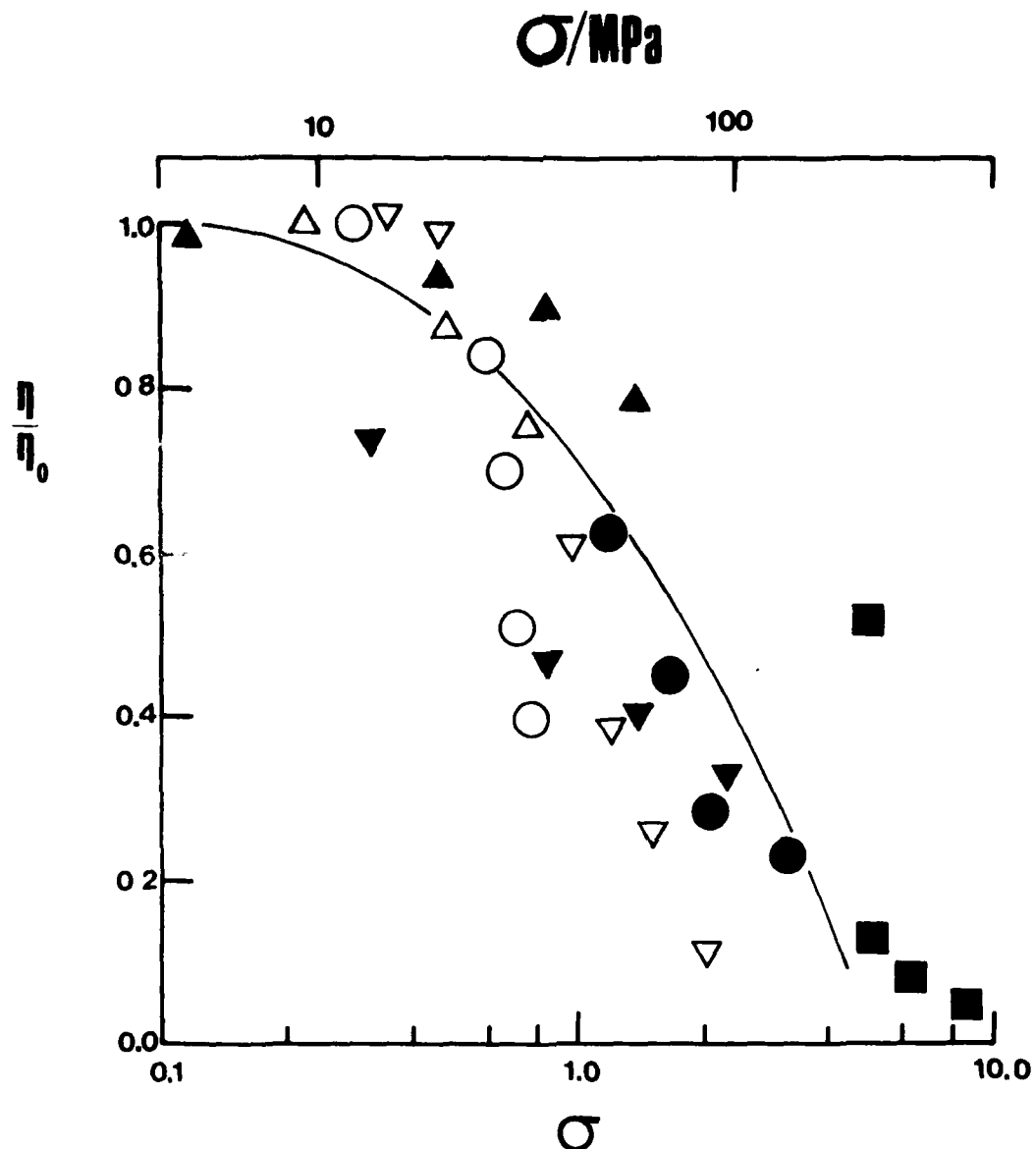


Figure A-2. The Nonlinear Behavior of: Δ BP L63/1271 ($P = 0.8 \text{ GPa}$, $T = 27^\circ\text{C}$, $U = 1.12 \text{ m/s}$), O 5P4E ($P = 0.45 \text{ GPa}$, $T = 27^\circ\text{C}$, $U = 0.6 \text{ m/s}$) and ∇ Oxitilube 85/140 ($P = 1.2 \text{ GPa}$, $T = 30^\circ\text{C}$, $U = 2.2 \text{ m/s}$) from Twin-Disk Experiments. The MHS Model: $\blacktriangle \rho = 0.8442$, $\blacktriangledown \rho = 0.92862$, $\bullet \rho = 1.01304$ and open square $\rho = 1.2663$.

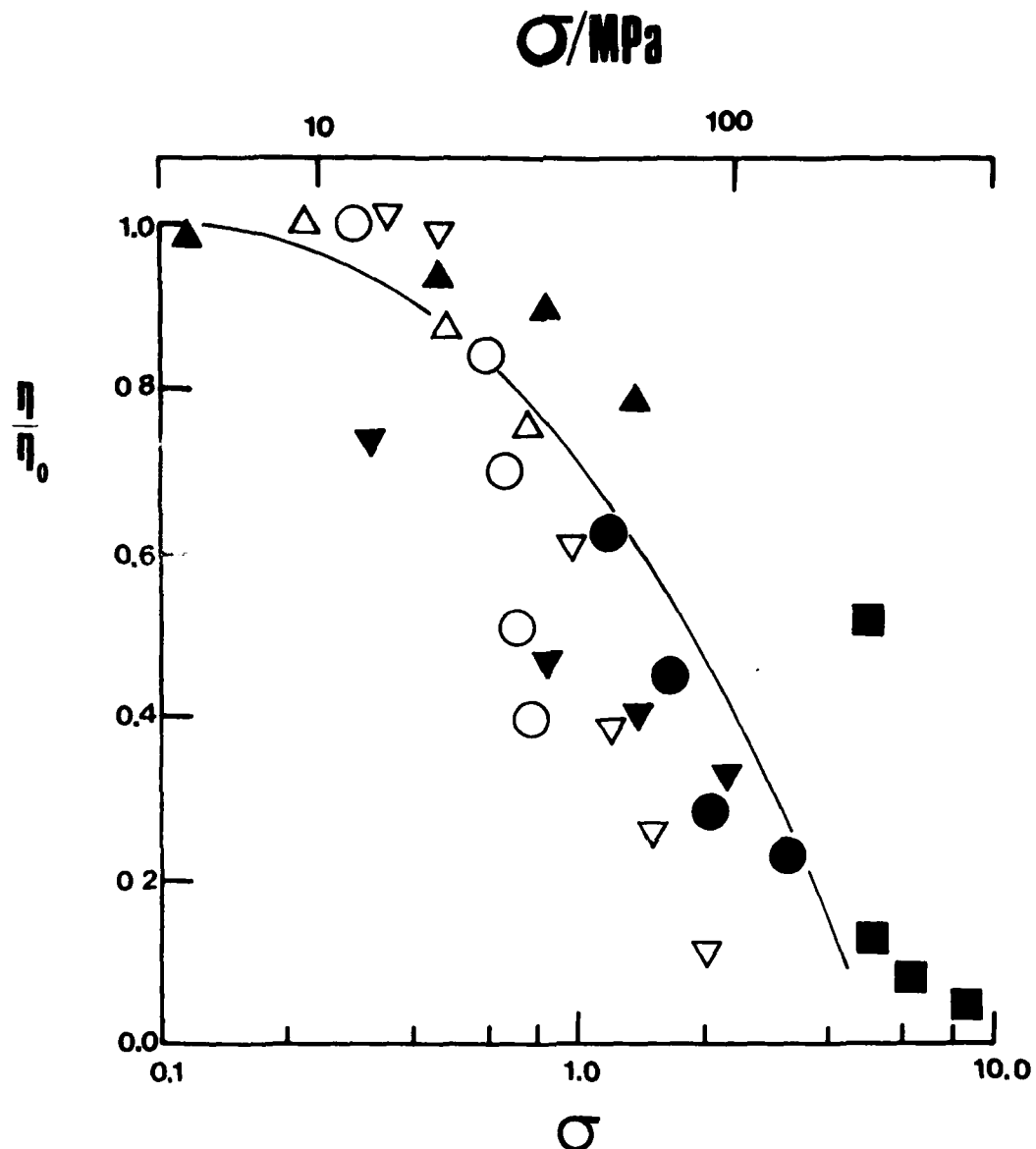


Figure A-2. The Nonlinear Behavior of: Δ BP L63/1271 ($P = 0.8 \text{ GPa}$, $T = 27^\circ\text{C}$, $U = 1.12 \text{ m/s}$), O 5P4E ($P = 0.45 \text{ GPa}$, $T = 27^\circ\text{C}$, $U = 0.6 \text{ m/s}$) and ∇ Oxitilube 85/140 ($P = 1.2 \text{ GPa}$, $T = 30^\circ\text{C}$, $U = 2.2 \text{ m/s}$) from Twin-Disk Experiments. The MHS Model: $\blacktriangle \rho = 0.8442$, $\blacktriangledown \rho = 0.92862$, $\bullet \rho = 1.01304$ and open square $\rho = 1.2663$.

CALCULATION OF SHEAR INDUCED STRUCTURAL CHANGES

The results in the previous section suggest that the model and real liquids might share a common mechanism of "failure" at high levels of shear stress. With the support of the previous results we now consider associated structural changes produced by the large shear rates in the fluids in order to better understand the failure mechanism.

A directional number density function, $n(\alpha)$, has been calculated for the purpose of investigating structural anisotropy. The function $n(x)$, for example, is the average number of molecules from a reference particle in the distance range $|x|$ to $|x| + \Delta x$, where Δx was taken as 1/200, selected from the N-1 particles in the re-oriented MD cell. Figure A-3 shows the $n(\alpha)$ of the unsheared liquid subtracted from that of the sheared system, $\delta n(\alpha)$. Although the maximum displacement is 10% at most, there is evidence of a tendency of the molecules to re-order themselves into xv layers (layers normal to the velocity gradient). The xz shearing increases the probability of the molecules in an xz plane being found at multiples of the intermolecular diameter from each other in the z direction. It is energetically favorable for these layers to be staggered in the y direction. Although not so well defined, these trends are present at the lower densities. The (grossly simplified) picture that emerges is one of corrugated sheets of atoms sliding past one another. A pictorial representation of this suggested structure is given in figure A-4. The structural reorganization results from the action of the imposed velocity profile which, at the shear rates considered, dominates the molecular motion. Major movements are confined to the line of shear.

Another aspect of the shear induced structural distortion is presented by the time dependent pair radial distribution function, $g(r,t)$, which is conveniently decomposed into the following component configurational averages:

$$\begin{aligned} g(r,t) &= g_0(r) + (x^2/r^2)u_{xx}(r,t) + (y^2/r^2)u_{yy}(r,t) \\ &\quad + (z^2/r^2)u_{zz}(r,t) + (xz/r^2)u_{xz}(r,t) \\ &= \dots, \end{aligned} \tag{3}$$

where $g_0(r)$ is the pair radial distribution function of the unsheared medium.

If $f_{\alpha\beta}(r,t)$ is the average of $\langle \alpha_{ij}\beta_{ij}/r_{ij}^2 \rangle$ in the radial element $r \rightarrow r + dr$ about a molecule i at time t , then

$$g_{\alpha\alpha}(r,t) = 15 f_{\alpha\alpha}(r,t) / (4\pi\rho r^2 dr),$$

and

$$g_{\alpha\beta}(r,t) = 15 f_{\alpha\beta}(r,t) / (4\pi\rho r^2 dr), \tag{4}$$

where $\alpha \neq \beta$

The $f_{\alpha\beta}(r,t)$ have been calculated at various times during the segment. The difference between the $g_{\alpha\alpha}(r,t)$ of the steady state sheared system and the unsheared system at the same density, $\delta g_{\alpha\alpha}(r,t)$, is shown in figure A-5. It reveals that shearing produces a net movement of particles in each coordination shell towards the origin molecule.

The shear rate dependent $g_{xz}(r,t)$ at steady state of the $\rho = 0.84$ system are compared with the spherically averaged $g(r,t)$ from these samples in figure A-6. They give convincing evidence of angular distortion in each coordination shell such that in the positive xz quadrants

CALCULATION OF SHEAR INDUCED STRUCTURAL CHANGES

The results in the previous section suggest that the model and real liquids might share a common mechanism of "failure" at high levels of shear stress. With the support of the previous results we now consider associated structural changes produced by the large shear rates in the fluids in order to better understand the failure mechanism.

A directional number density function, $n(\alpha)$, has been calculated for the purpose of investigating structural anisotropy. The function $n(x)$, for example, is the average number of molecules from a reference particle in the distance range $|x|$ to $|x| + \Delta x$, where Δx was taken as 1/200, selected from the N-1 particles in the re-oriented MD cell. Figure A-3 shows the $n(\alpha)$ of the unsheared liquid subtracted from that of the sheared system, $\delta n(\alpha)$. Although the maximum displacement is 10% at most, there is evidence of a tendency of the molecules to re-order themselves into xv layers (layers normal to the velocity gradient). The xz shearing increases the probability of the molecules in an xz plane being found at multiples of the intermolecular diameter from each other in the z direction. It is energetically favorable for these layers to be staggered in the y direction. Although not so well defined, these trends are present at the lower densities. The (grossly simplified) picture that emerges is one of corrugated sheets of atoms sliding past one another. A pictorial representation of this suggested structure is given in figure A-4. The structural reorganization results from the action of the imposed velocity profile which, at the shear rates considered, dominates the molecular motion. Major movements are confined to the line of shear.

Another aspect of the shear induced structural distortion is presented by the time dependent pair radial distribution function, $g(r,t)$, which is conveniently decomposed into the following component configurational averages:

$$\begin{aligned} g(r,t) &= g_0(r) + (x^2/r^2)u_{xx}(r,t) + (y^2/r^2)u_{yy}(r,t) \\ &\quad + (z^2/r^2)u_{zz}(r,t) + (xz/r^2)u_{xz}(r,t) \\ &= \dots, \end{aligned} \tag{3}$$

where $g_0(r)$ is the pair radial distribution function of the unsheared medium.

If $f_{\alpha\beta}(r,t)$ is the average of $\langle \alpha_{ij}\beta_{ij}/r_{ij}^2 \rangle$ in the radial element $r \rightarrow r + dr$ about a molecule i at time t , then

$$g_{\alpha\alpha}(r,t) = 15 f_{\alpha\alpha}(r,t) / (4\pi\rho r^2 dr),$$

and

$$g_{\alpha\beta}(r,t) = 15 f_{\alpha\beta}(r,t) / (4\pi\rho r^2 dr), \tag{4}$$

where $\alpha \neq \beta$

The $f_{\alpha\beta}(r,t)$ have been calculated at various times during the segment. The difference between the $g_{\alpha\alpha}(r,t)$ of the steady state sheared system and the unsheared system at the same density, $\delta g_{\alpha\alpha}(r,t)$, is shown in figure A-5. It reveals that shearing produces a net movement of particles in each coordination shell towards the origin molecule.

The shear rate dependent $g_{xz}(r,t)$ at steady state of the $\rho = 0.84$ system are compared with the spherically averaged $g(r,t)$ from these samples in figure A-6. They give convincing evidence of angular distortion in each coordination shell such that in the positive xz quadrants

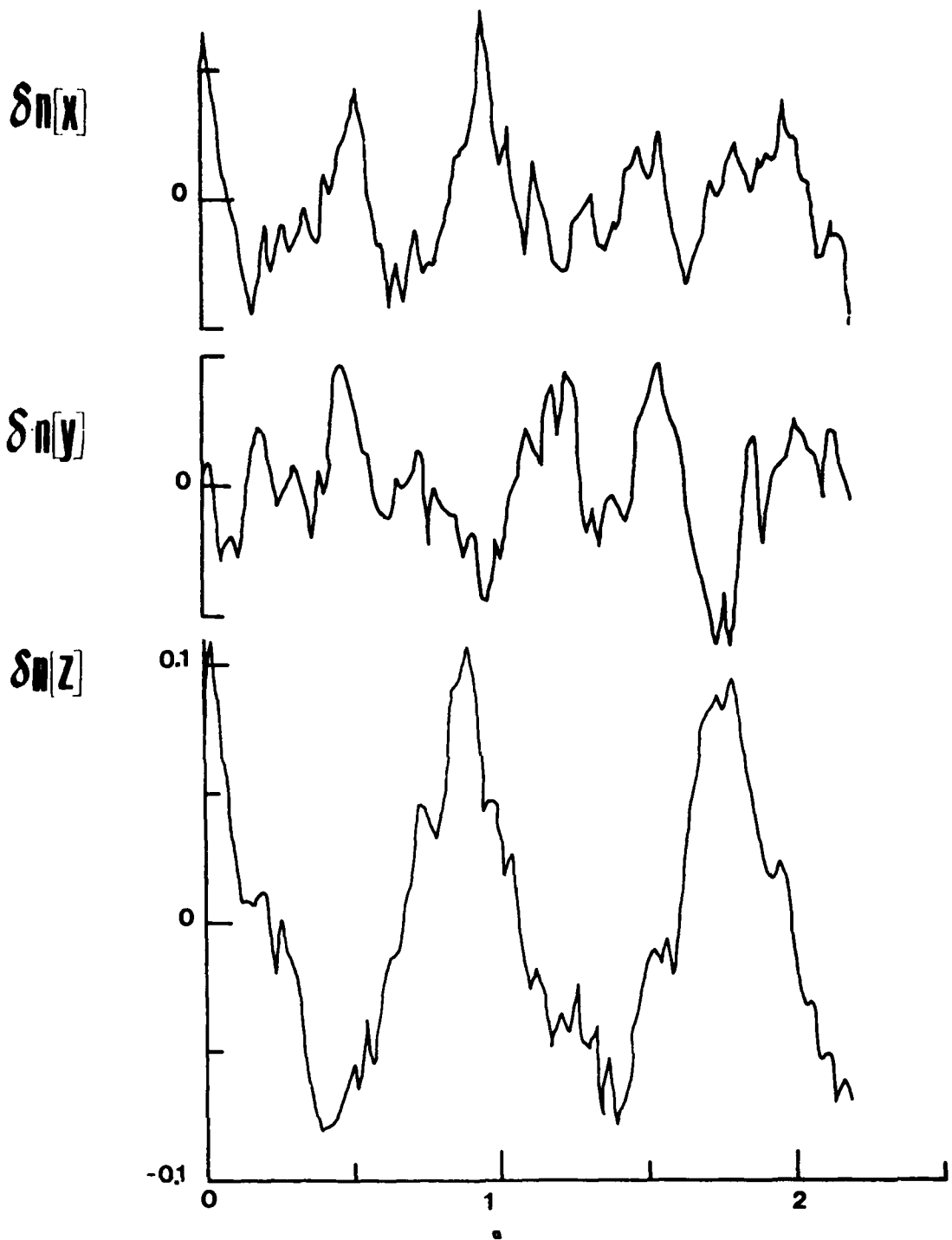


Figure A-3. The Excess Directional-Number-Density Functions, $\delta n(\alpha)$, for the $\rho = 1.2663$ and $i_{xz} = 0.7721$ State.

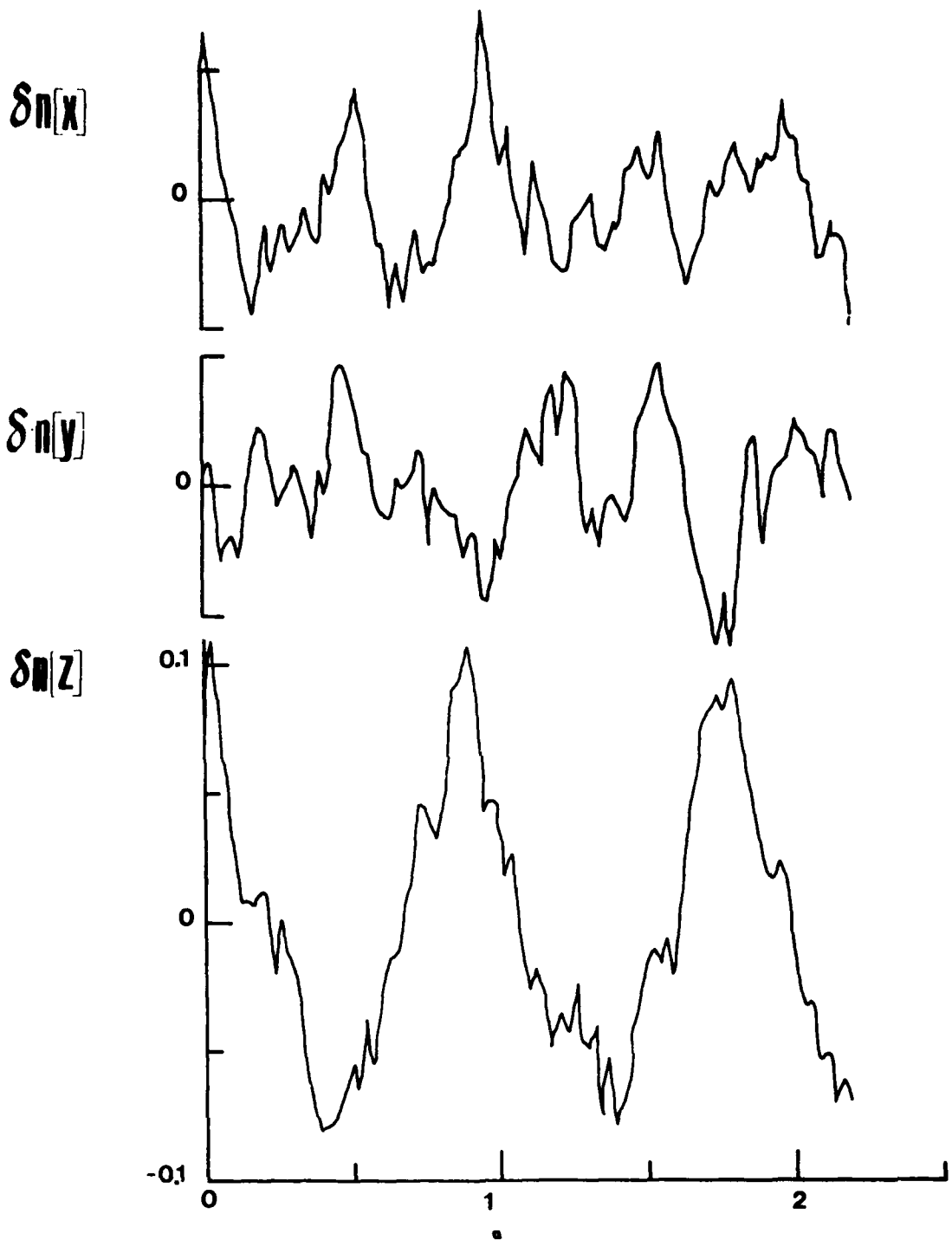


Figure A-3. The Excess Directional-Number-Density Functions, $\delta n(\alpha)$, for the $\rho = 1.2663$ and $i_{xz} = 0.7721$ State.

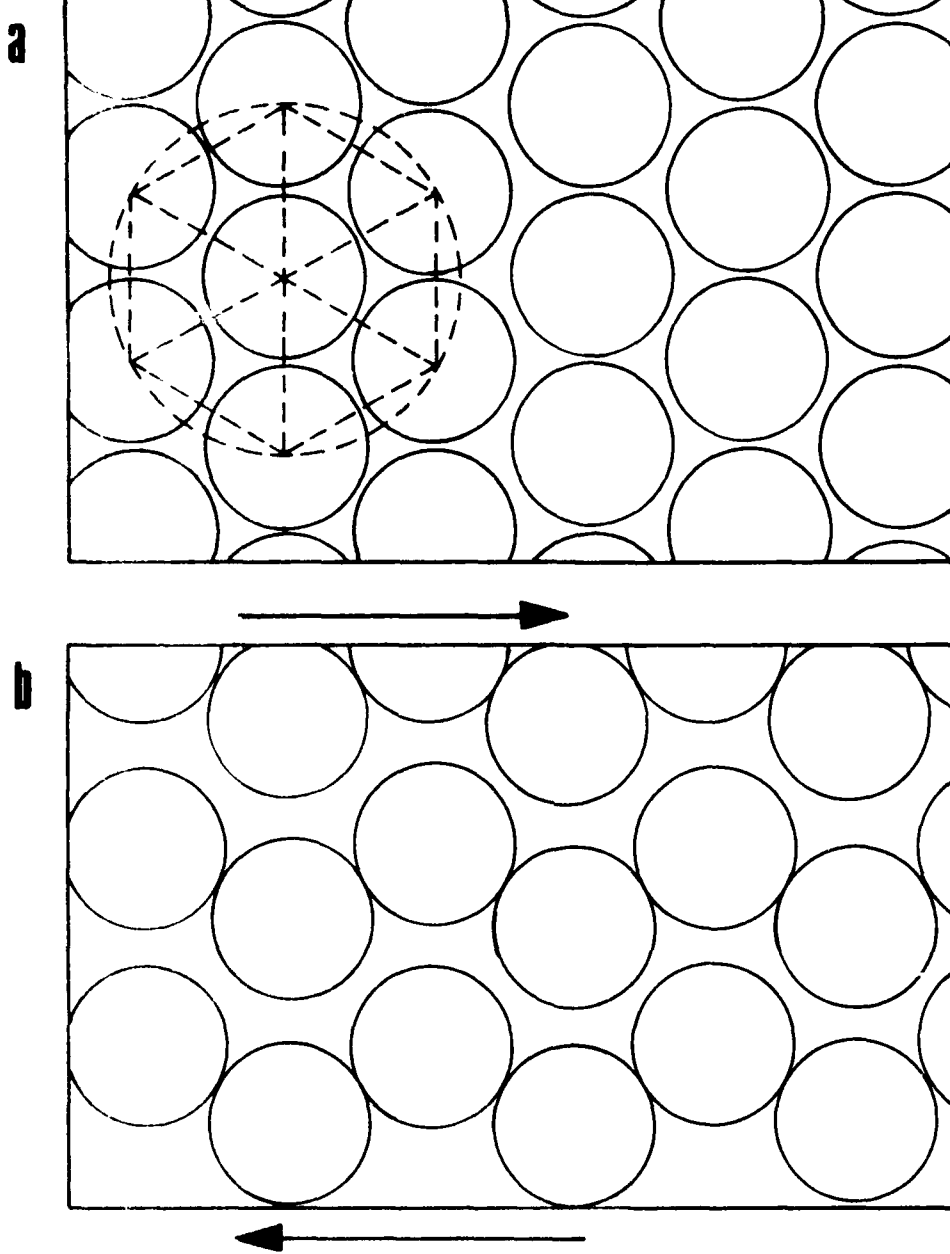


Figure A-4. A Pictorial Representation of the Structural Changes That Take Place on Going from an Unsheared (a) to a Sheared (b) State. The arrows denote the line and plane of shear.

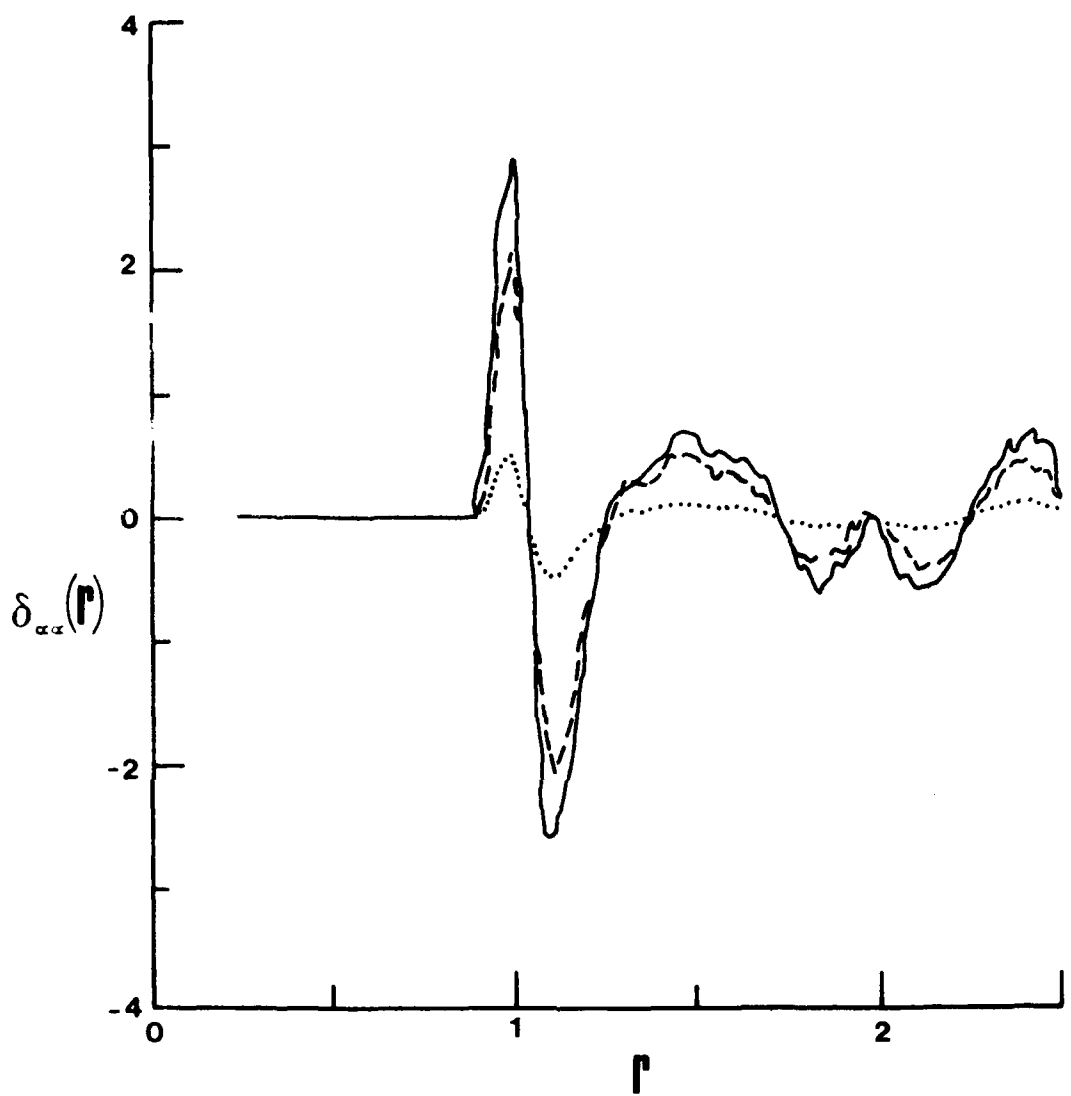


Figure A-5. The $g(r)$, $g_{xx}(r)$ _____, and $g_{yy}(r)$ _____, of the Sheared Minus the Unsheared Portions of the $\rho = 1.01304$ and $\dot{\epsilon}_{xz} = 0.7168$ Segmented Calculation.

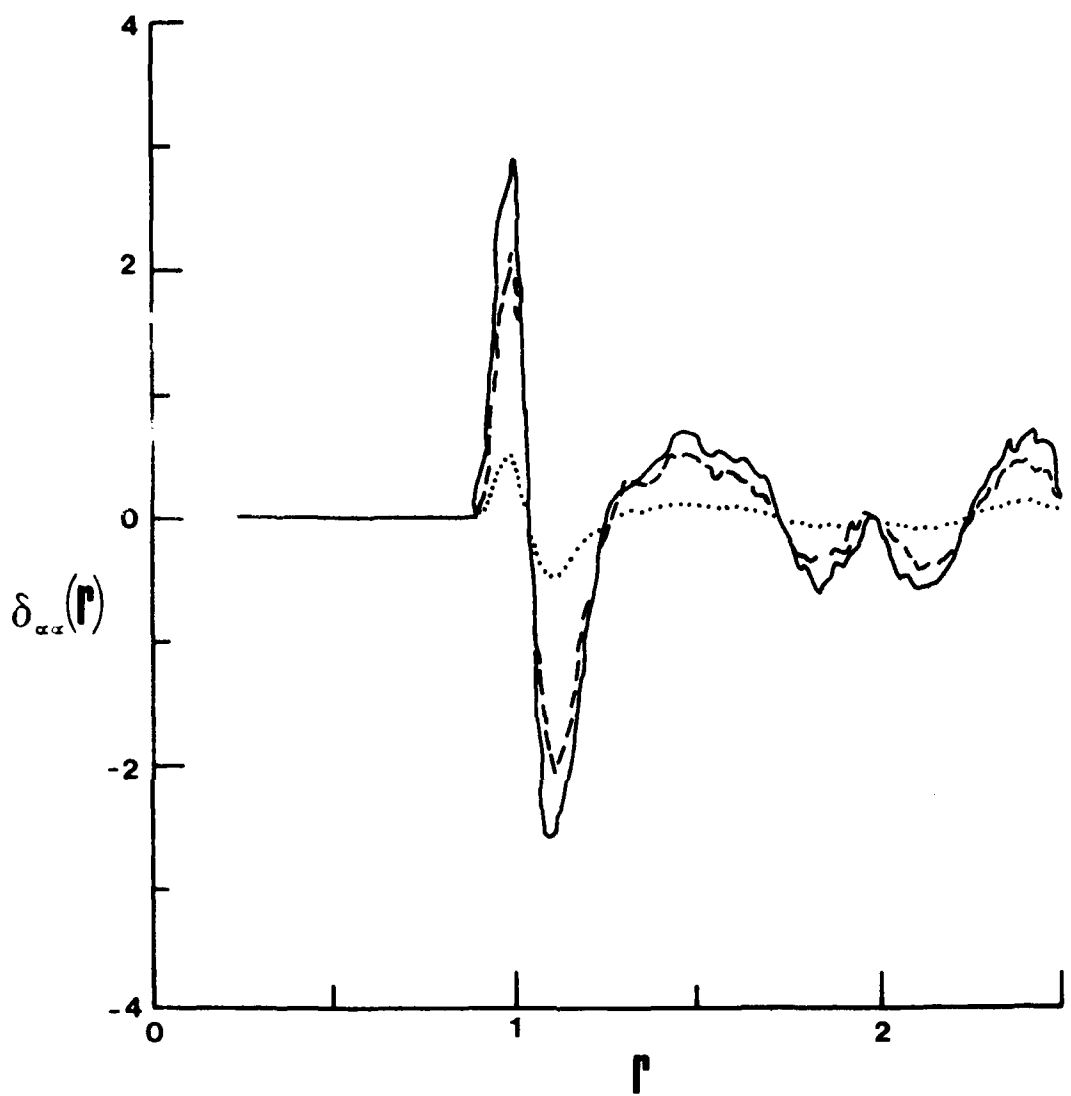


Figure A-5. The $g(r)$, $g_{xx}(r)$ _____, and $g_{yy}(r)$ _____, of the Sheared Minus the Unsheared Portions of the $\rho = 1.01304$ and $\dot{\epsilon}_{xz} = 0.7168$ Segmented Calculation.

the inside of each shell is on average depleted of particles when compared with the unsheared liquid. In contrast, the outside of each shell has an excess of molecules in the positive xz quadrants, when compared with the unsheared medium. The opposite changes take place in the negative quadrants.

EFFECT OF STRUCTURAL REORGANIZATION ON MOLECULAR MOBILITY

It is to be expected that the effect of the shear should not be confined to structural changes but must also alter the self-diffusional dynamics of the molecules. To assess this, the x , y , and z components of the mean square displacements, $\langle r_\alpha^2(t) \rangle$, which exclude the imposed flow, have been calculated, i.e.,

$$\langle r_\alpha^2(t) \rangle = \sum_i^N \left\langle \left[\int_0^t v_i^\alpha(t') dt' - \alpha_i(0) \right]^2 \right\rangle / N. \quad (5)$$

The directional diffusion coefficients,

$$D_\alpha = \frac{1}{2} \left[\frac{d \langle r_\alpha^2(t \rightarrow \infty) \rangle}{dt} \right],$$

A selection of the states are presented table A-2. The value of $D_\alpha = 0.032$ for the unsheared liquid near the triple point compares favorably with the equilibrium value of 0.033. The D_α of the unsheared liquid decrease by approximately an order of magnitude on increasing the density from $\rho = 0.8442$ to 1.2663 . However, at larger shear rates the density has a diminishing influence on the diffusion coefficients. The high shear stresses enhance the fluidity and create a "liquid" which has directionality. All the diffusion coefficient components rise with shear rate at a particular density because the structural reorganization that takes place on shearing apparently creates paths along which particles can move more readily. The D_y are typically two-thirds of the D_x and D_z , indicating that the self-diffusion is favored in the shearing plane. Thus, paradoxically, although structural aspects of the liquids under shear present a more solid-like appearance, other more dynamically related properties such as self-diffusion and shear viscosity manifest changes which are associated with enhanced fluidity.

Thus we see that the high stresses cause extreme distortions of the system's structure. The intermolecular forces are not sufficiently strong to support the enormous stress levels that develop; consequently there is a rupturing and reorganization of the structure resulting in enhanced flow behavior, due to the alignment of molecules into "glide" planes along the line of shear.

These structural rearrangements are also manifest in changes in the so-called normal pressure components, $P_{\alpha\alpha}$ ($= -\sigma_{\alpha\alpha}$). Typically, $P_{zz} > P_{xx} > P_{yy}$ although their differences are small when compared with each component's change on shearing. In figure A-7 the time dependence of the increase in $P_{\alpha\alpha}(t)$ is shown. It is found that the time scale of the development of the normal pressure components is longer than that of the shear stress.

The difference in the viscoelastic and structural reorganization times can be better understood by further consideration of the radial distribution functions.

The time dependence of $g_{\alpha\alpha}(r,t)$ and $g_{\alpha\beta}(r,t)$ reveal that structural reorganization having the symmetry of shear, $\langle xz/r^2 \rangle$, is much faster than that of $\langle z^2/r^2 \rangle$ symmetry. Within the latter series, $\langle x^2/r^2 \rangle$ and $\langle z^2/r^2 \rangle$ evolve more rapidly to their steady state values than $\langle y^2/r^2 \rangle$. For example, when $\rho = 1.01304$ and $\epsilon_{xz} = 0.7168$, the former three averages have

the inside of each shell is on average depleted of particles when compared with the unsheared liquid. In contrast, the outside of each shell has an excess of molecules in the positive xz quadrants, when compared with the unsheared medium. The opposite changes take place in the negative quadrants.

EFFECT OF STRUCTURAL REORGANIZATION ON MOLECULAR MOBILITY

It is to be expected that the effect of the shear should not be confined to structural changes but must also alter the self-diffusional dynamics of the molecules. To assess this, the x , y , and z components of the mean square displacements, $\langle r_\alpha^2(t) \rangle$, which exclude the imposed flow, have been calculated, i.e.,

$$\langle r_\alpha^2(t) \rangle = \sum_i^N \left\langle \left[\int_0^t v_i^\alpha(t') dt' - \alpha_i(0) \right]^2 \right\rangle / N. \quad (5)$$

The directional diffusion coefficients,

$$D_\alpha = \frac{1}{2} \left[\frac{d \langle r_\alpha^2(t \rightarrow \infty) \rangle}{dt} \right],$$

A selection of the states are presented table A-2. The value of $D_\alpha = 0.032$ for the unsheared liquid near the triple point compares favorably with the equilibrium value of 0.033. The D_α of the unsheared liquid decrease by approximately an order of magnitude on increasing the density from $\rho = 0.8442$ to 1.2663 . However, at larger shear rates the density has a diminishing influence on the diffusion coefficients. The high shear stresses enhance the fluidity and create a "liquid" which has directionality. All the diffusion coefficient components rise with shear rate at a particular density because the structural reorganization that takes place on shearing apparently creates paths along which particles can move more readily. The D_y are typically two-thirds of the D_x and D_z , indicating that the self-diffusion is favored in the shearing plane. Thus, paradoxically, although structural aspects of the liquids under shear present a more solid-like appearance, other more dynamically related properties such as self-diffusion and shear viscosity manifest changes which are associated with enhanced fluidity.

Thus we see that the high stresses cause extreme distortions of the system's structure. The intermolecular forces are not sufficiently strong to support the enormous stress levels that develop; consequently there is a rupturing and reorganization of the structure resulting in enhanced flow behavior, due to the alignment of molecules into "glide" planes along the line of shear.

These structural rearrangements are also manifest in changes in the so-called normal pressure components, $P_{\alpha\alpha}$ ($= -\sigma_{\alpha\alpha}$). Typically, $P_{zz} > P_{xx} > P_{yy}$ although their differences are small when compared with each component's change on shearing. In figure A-7 the time dependence of the increase in $P_{\alpha\alpha}(t)$ is shown. It is found that the time scale of the development of the normal pressure components is longer than that of the shear stress.

The difference in the viscoelastic and structural reorganization times can be better understood by further consideration of the radial distribution functions.

The time dependence of $g_{\alpha\alpha}(r,t)$ and $g_{\alpha\beta}(r,t)$ reveal that structural reorganization having the symmetry of shear, $\langle xz/r^2 \rangle$, is much faster than that of $\langle z^2/r^2 \rangle$ symmetry. Within the latter series, $\langle x^2/r^2 \rangle$ and $\langle z^2/r^2 \rangle$ evolve more rapidly to their steady state values than $\langle y^2/r^2 \rangle$. For example, when $\rho = 1.01304$ and $\epsilon_{xz} = 0.7168$, the former three averages have

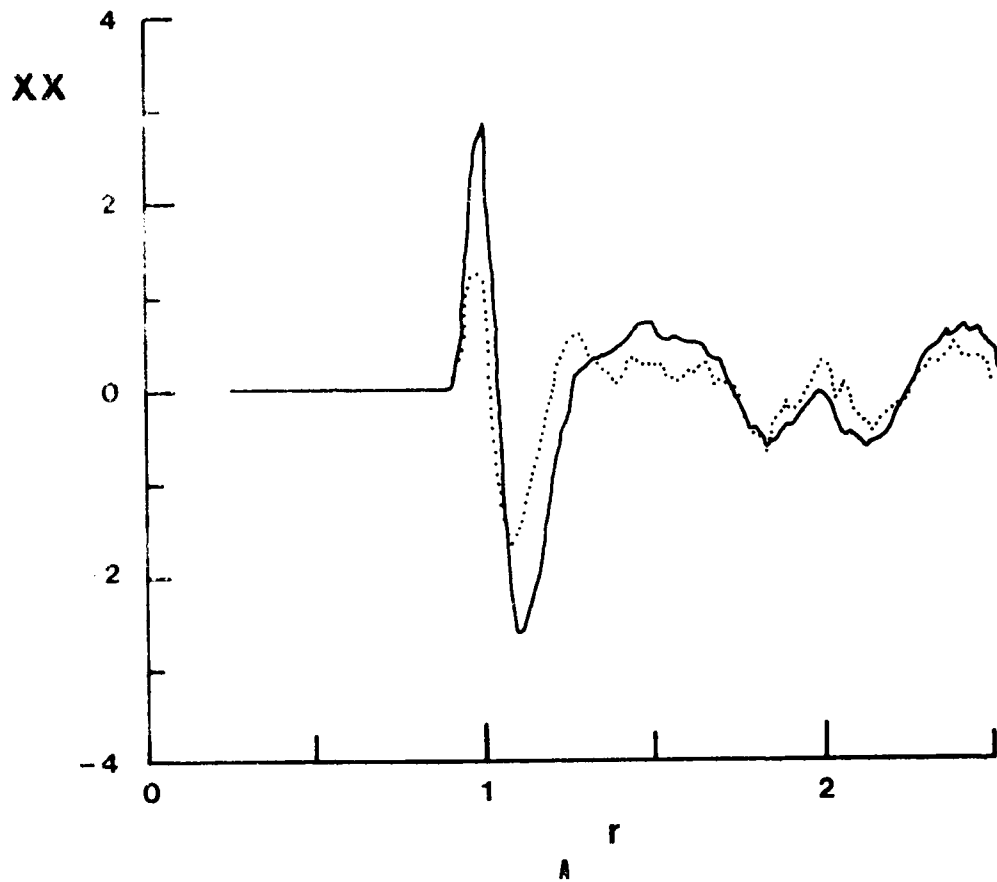


Figure A-6. The Difference Between the Equilibrium and Sheared Coefficients [(a) g_{xx} , (b) g_{yy} , (c) g_{zz} , (d) g_{xz}] for the Same State and Shear History as in Fig. A-5. The Solid Curve is for $t = 1.8$ and the Dotted Curve is for $t = .4$.

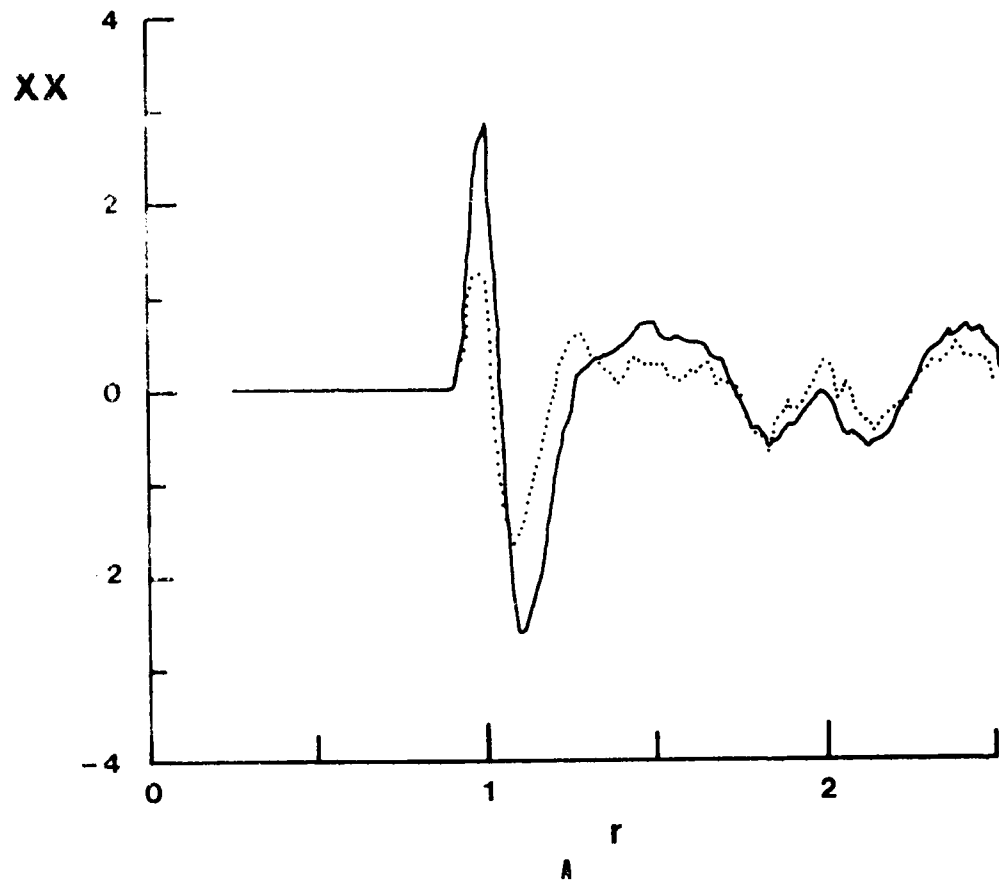


Figure A-6. The Difference Between the Equilibrium and Sheared Coefficients [(a) g_{xx} , (b) g_{yy} , (c) g_{zz} , (d) g_{xz}] for the Same State and Shear History as in Fig. A-5. The Solid Curve is for $t = 1.8$ and the Dotted Curve is for $t = .4$.

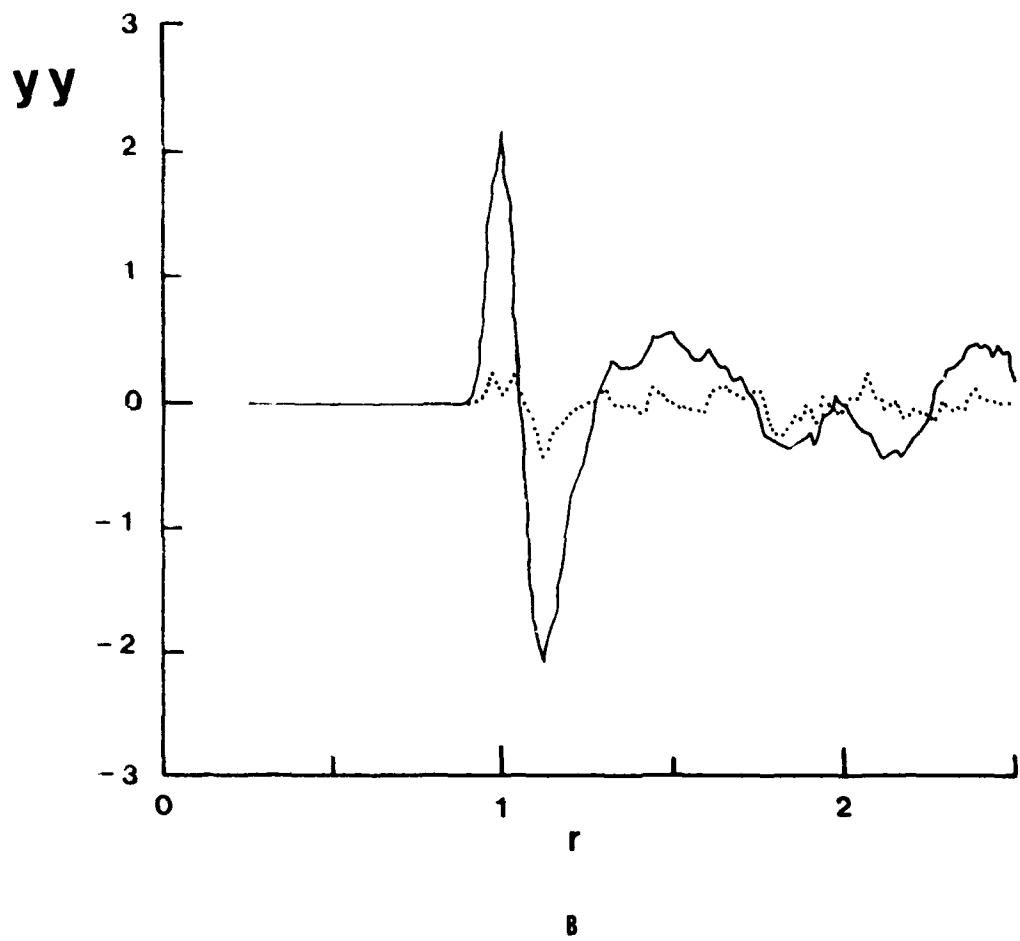


Figure A-6. Contd.

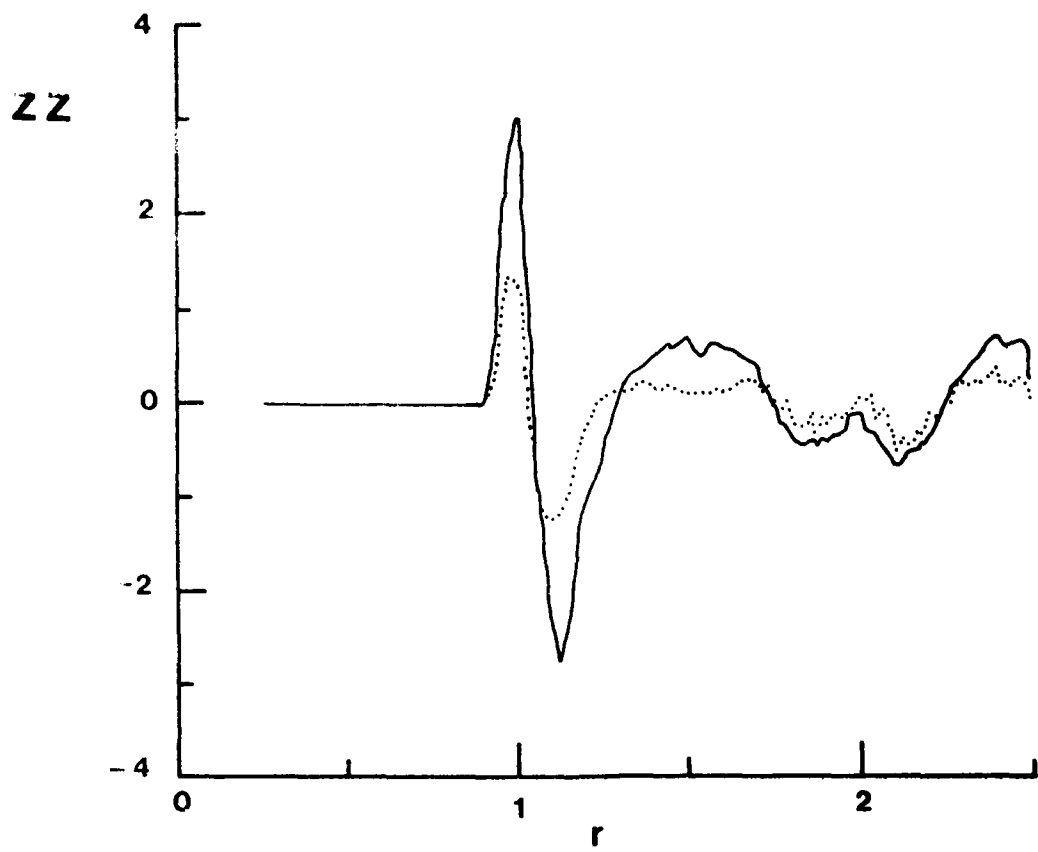


Figure A-6. Contd.

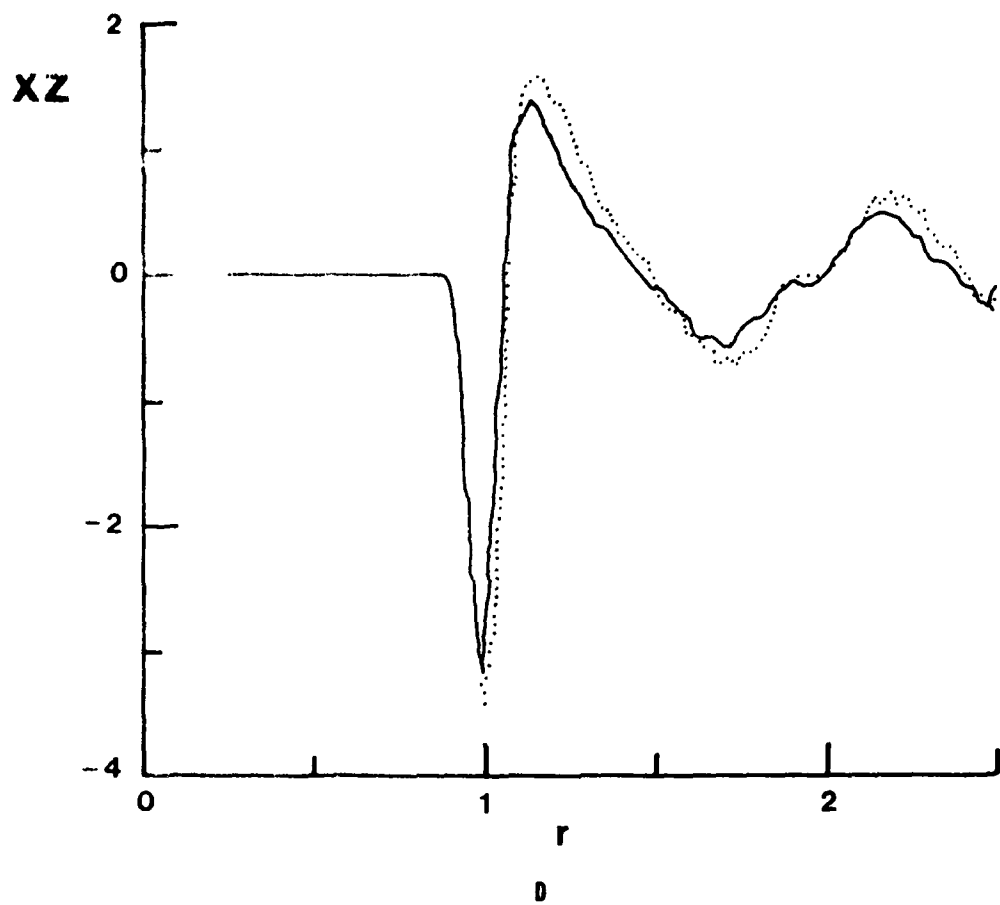


Figure A-6. Contd.

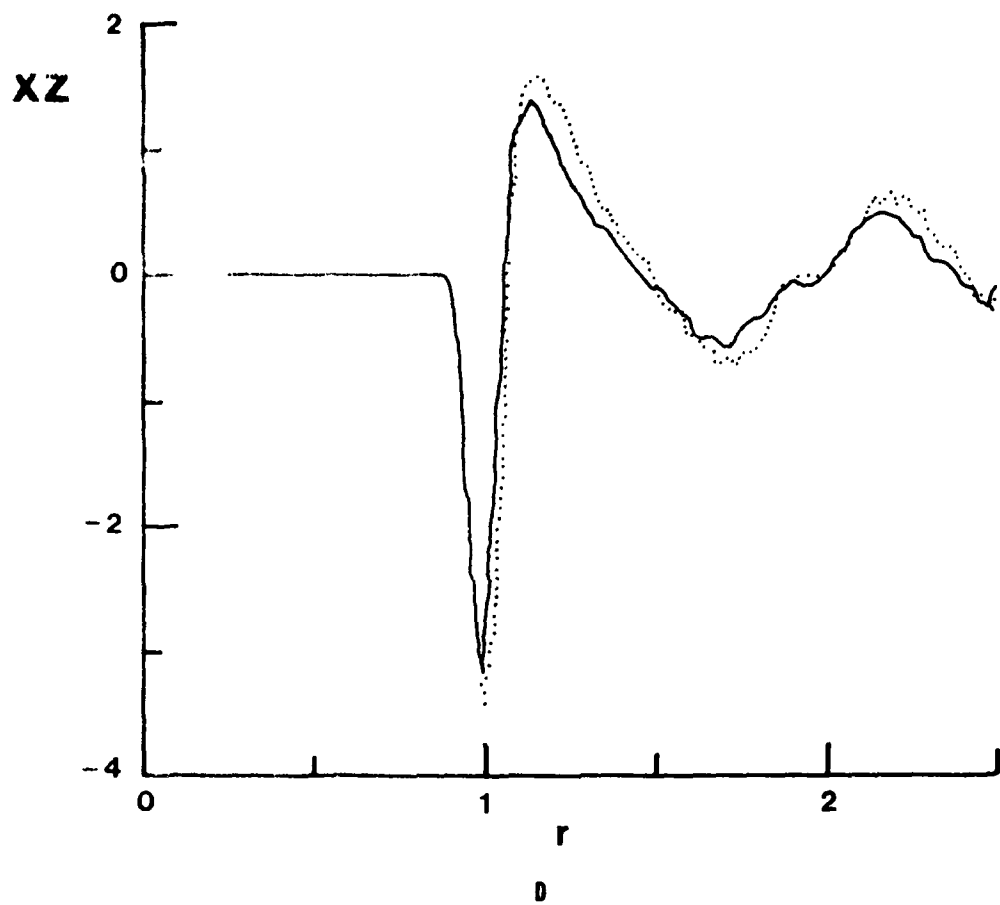


Figure A-6. Contd.

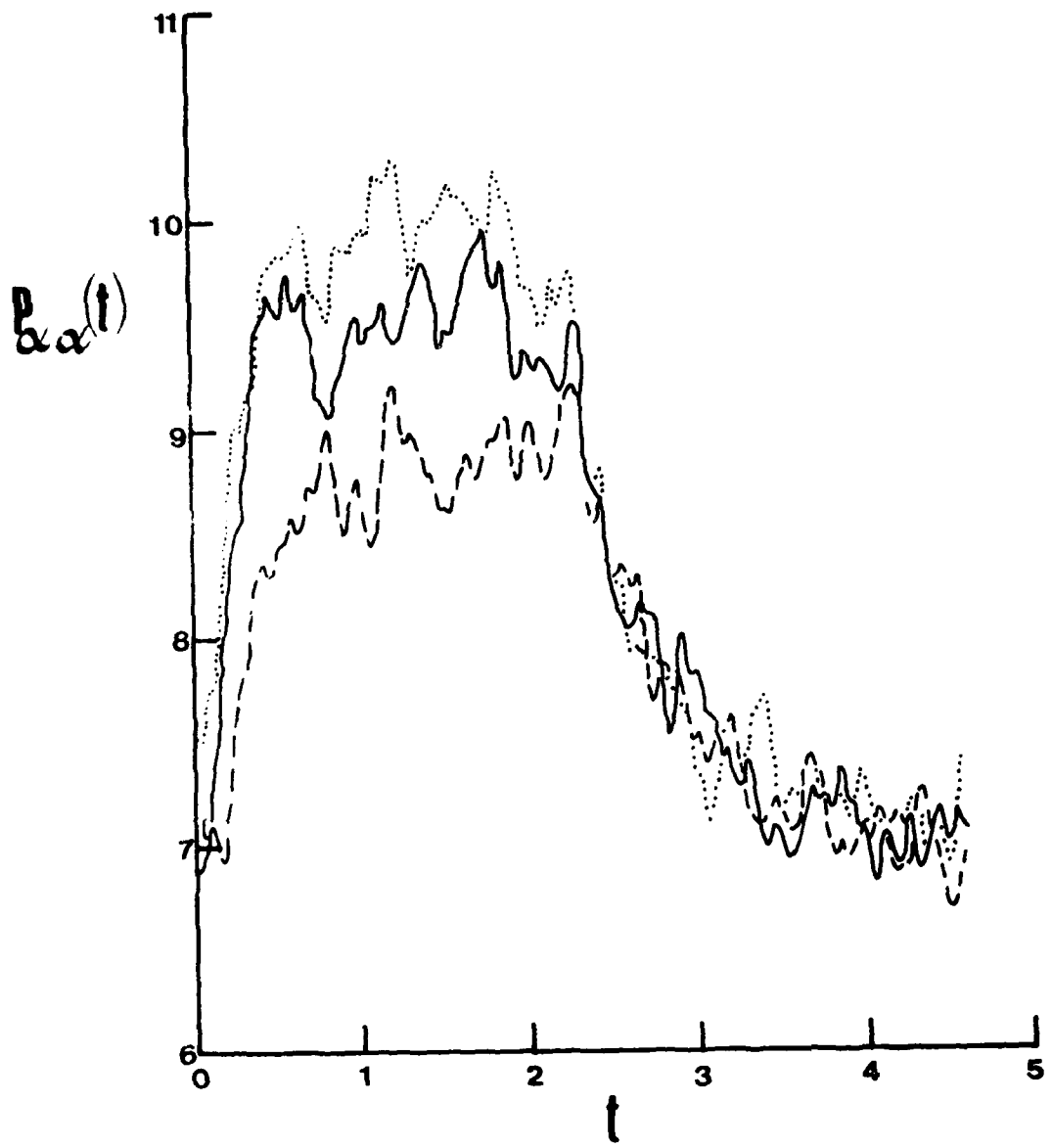


Figure A.7. The Time-Dependent Normal Pressure Components for the Strain Rate History.
 $\dot{\epsilon} = 0.7168$, $\rho = 1.01304$. ρ , _____ $p_{xx}(t)$, _____ $p_{yy}(t)$, and $p_{zz}(t)$

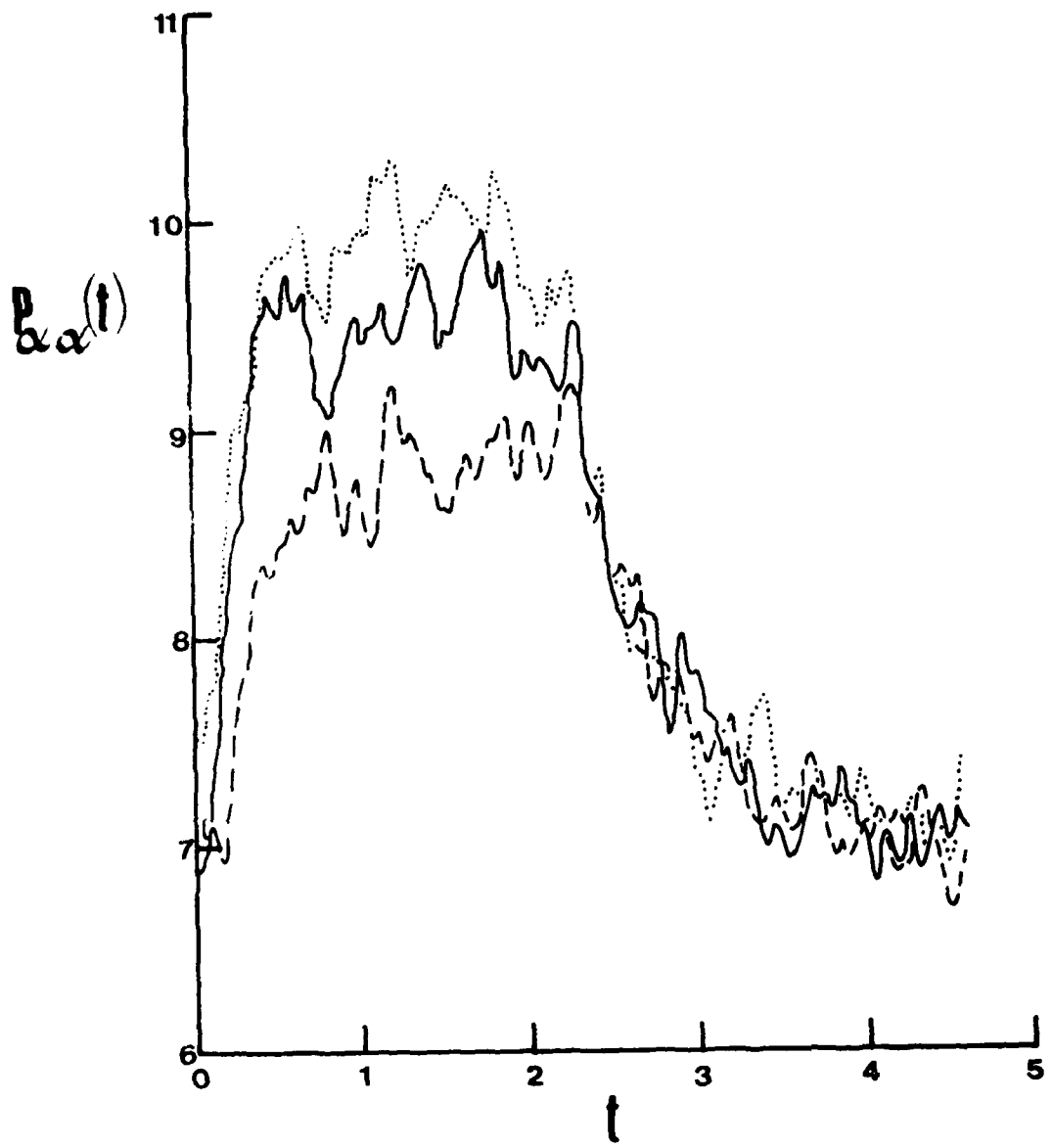


Figure A.7. The Time-Dependent Normal Pressure Components for the Strain Rate History.
 $\dot{\epsilon} = 0.7168$, $\rho = 1.01304$. ρ , _____ $p_{xx}(t)$, _____ $p_{yy}(t)$, and $p_{zz}(t)$

nearly reached their steady state values by $t = 0.25$ whereas that of the $\langle y^2/r^2 \rangle$ summation hardly differs from zero by that time. Thus we find that when a liquid is sheared, the shearing forces alter its structure so that the steady state stress attained corresponds to a new lower viscosity, not that characterizing the starting liquid. At high rates of shear the structural evolution necessary to attain this new viscosity is significantly slower than the viscoelastic shear relaxation. Viewed simply this means that the original viscosity can remain for a sufficiently long time to enable the shear stress to exceed its steady state value.

Table A-2. The Density and Shear Rate Dependence of the Directional Diffusion Coefficients, D_α , Obtained from the MD Experiments.

ρ	$\dot{\epsilon}_{xz}$	D_x	D_y	D_z
0.84	0.0	0.032	0.032	0.032
0.84	0.67	0.052	0.045	0.052
0.93	0.0	0.018	0.018	0.018
0.93	0.69	0.043	0.037	0.045

It has come to be increasingly recognized that the process of fracture involves time dependent nonlinear viscoelastic behavior. In order to better understand the time dependent nonlinear viscoelasticity, the MD calculations were conducted with a time varying strain rate. In what follows we describe the viscoelastic MD "experiments" and the results. What is most encouraging is that in every case the behavior of real liquids is mimicked by the MD results.

We consider the dynamical response of the LJ material to an imposed shear that is "switched on" suddenly using the Homogeneous Shear method. Two types of MD experiments are of interest: (a) the response of the system to a steady shearing rate (uniform velocity gradient) $\dot{\epsilon} = \partial v_x / \partial z$ that is initiated at time $t = 0$; and (b) the response of the system to a constant shear strain (a pulse of shearing rate) imposed at time $t = t'$. Linear response theory provides us with relations between the two types of responses: the shear stress response to a step of shear strain can be written as

$$\sigma(t)/\dot{\epsilon} = G_\infty \phi(t), \quad (6)$$

where $\phi(t)$ is the normalized ($\phi(0) = 1$) shear stress relaxation function. In terms of these parameters the shear stress response to a "small" steady shear rate imposed at $t = 0$ is,

$$\sigma(t)/\dot{\epsilon} = G_\infty \int_0^t dt' \phi(t'). \quad (7)$$

Since the steady state ($t \rightarrow \infty$) value of this is just the viscosity of the material, η_0 , we have,

$$\eta_0 = G_\infty \int_0^\infty dt' \phi(t') = G_\infty \tau. \quad (8)$$

The last equality serves to define the shear realization time τ .

nearly reached their steady state values by $t = 0.25$ whereas that of the $\langle y^2/r^2 \rangle$ summation hardly differs from zero by that time. Thus we find that when a liquid is sheared, the shearing forces alter its structure so that the steady state stress attained corresponds to a new lower viscosity, not that characterizing the starting liquid. At high rates of shear the structural evolution necessary to attain this new viscosity is significantly slower than the viscoelastic shear relaxation. Viewed simply this means that the original viscosity can remain for a sufficiently long time to enable the shear stress to exceed its steady state value.

Table A-2. The Density and Shear Rate Dependence of the Directional Diffusion Coefficients, D_α , Obtained from the MD Experiments.

ρ	$\dot{\epsilon}_{xz}$	D_x	D_y	D_z
0.84	0.0	0.032	0.032	0.032
0.84	0.67	0.052	0.045	0.052
0.93	0.0	0.018	0.018	0.018
0.93	0.69	0.043	0.037	0.045

It has come to be increasingly recognized that the process of fracture involves time dependent nonlinear viscoelastic behavior. In order to better understand the time dependent nonlinear viscoelasticity, the MD calculations were conducted with a time varying strain rate. In what follows we describe the viscoelastic MD "experiments" and the results. What is most encouraging is that in every case the behavior of real liquids is mimicked by the MD results.

We consider the dynamical response of the LJ material to an imposed shear that is "switched on" suddenly using the Homogeneous Shear method. Two types of MD experiments are of interest: (a) the response of the system to a steady shearing rate (uniform velocity gradient) $\dot{\epsilon} = \partial v_x / \partial z$ that is initiated at time $t = 0$; and (b) the response of the system to a constant shear strain (a pulse of shearing rate) imposed at time $t = t'$. Linear response theory provides us with relations between the two types of responses: the shear stress response to a step of shear strain can be written as

$$\sigma(t)/\dot{\epsilon} = G_\infty \phi(t), \quad (6)$$

where $\phi(t)$ is the normalized ($\phi(0) = 1$) shear stress relaxation function. In terms of these parameters the shear stress response to a "small" steady shear rate imposed at $t = 0$ is,

$$\sigma(t)/\dot{\epsilon} = G_\infty \int_0^t dt' \phi(t'). \quad (7)$$

Since the steady state ($t \rightarrow \infty$) value of this is just the viscosity of the material, η_0 , we have,

$$\eta_0 = G_\infty \int_0^\infty dt' \phi(t') = G_\infty \tau. \quad (8)$$

The last equality serves to define the shear realization time τ .

Experiments of the type described as (a) above were then carried out as a function of $\dot{\epsilon}$ for values of $\dot{\epsilon}$ well beyond the range for which linear behavior can be expected. A representative selection of the results is displayed in figures A-8 and A-9 in which the density (constant $\dot{\epsilon}$) and shear rate (constant density) dependence of η are shown, respectively.

Several features of these figures are worthy of comment. At short times the system behaves largely as an elastic solid in that the stress increases linearly with time,

$$\sigma(t) = G_\infty \dot{\epsilon} t. \quad (9)$$

The shear rigidity modulus rises linearly with pressure at roughly the same rate as more complicated fluids, as is revealed in figure A-10. Liquids cannot permanently support a shear strain and consequently the stress levels off to a value determined by the shear viscosity of the sheared state. There is evident "shear thinning," or a decrease of viscosity with increasing shear rate. The predicted value of the stress build-up for the $\rho = 0.92862$, $\dot{\epsilon} = 0.6963$ state using equation (7), shown in figure A-8, clearly overestimates the actual stress obtained.

Also, a maximum in the stress versus time curve for those simulations in the high density/shear rate regime is observed. This indicates that the large shear deformations are producing structural distortions which lag in time somewhat behind the growth of the shear stress but follow rather closely the observed time variation of the normal pressure components in the material. This relatively slower development of what can be thought of as transient stress-induced glide planes is consistent with the observed shear thinning and stress "overshoot" behavior presented. It is also consistent with the observation that the stress relaxation function decays more rapidly in a highly sheared system than in an equilibrium system (see discussion of $g_{\text{eq}}\beta(t)$ above). A comparison of the two types of behavior is presented in figure A-11. The form of these $\phi(t)$ consists of a rapidly ($t < 0.2$) decaying portion which is presumably inertial in origin and due to small motions of the molecules within the random network structure. Further stress relaxation requires the cooperative rearrangement of larger molecular groups and is consequently slower. The attenuation of $\phi(t)$ with increasing shear rate is indicative of the enhanced stress relieving properties of the structurally reorganized system. The stress overshoot observed in nonlinear viscoelastic experiments on polymers has a form that is quite similar to the curves obtained for the LJ system. While the microscopic mechanisms for the two systems are obviously quite different, the general principle that associates the stress overshoot phenomena (as well as shear thinning) with a time dependent structural reorganization process remains quite valid.

In this context it is perhaps relevant to note that a more rapid decay of the stress relaxation function can be thought of as both a suppression of the long relaxation times associated with stress relaxation and also a reduction in the shear rigidity modulus, at low frequencies, G , (a rather well known phenomenon in polymeric systems).*

Thus we see that the viscoelastic studies at high shear rates reflect the structural reorganization that is ultimately responsible for failure or fracture of the liquid. The fact that every property "measured" at high shear rates are found in real and far more complicated liquids suggests strongly that MD studies can be utilized to investigate the comminution process in those liquids.

* Y. G. Yanovski in *Relaxation Phenomena in Polymers*, ed. G. Bartenev and Y. V. Zelenov (Khimiya, Leningrad, 1972), p. 113.

Experiments of the type described as (a) above were then carried out as a function of $\dot{\epsilon}$ for values of $\dot{\epsilon}$ well beyond the range for which linear behavior can be expected. A representative selection of the results is displayed in figures A-8 and A-9 in which the density (constant $\dot{\epsilon}$) and shear rate (constant density) dependence of η are shown, respectively.

Several features of these figures are worthy of comment. At short times the system behaves largely as an elastic solid in that the stress increases linearly with time,

$$\sigma(t) = G_\infty \dot{\epsilon} t. \quad (9)$$

The shear rigidity modulus rises linearly with pressure at roughly the same rate as more complicated fluids, as is revealed in figure A-10. Liquids cannot permanently support a shear strain and consequently the stress levels off to a value determined by the shear viscosity of the sheared state. There is evident "shear thinning," or a decrease of viscosity with increasing shear rate. The predicted value of the stress build-up for the $\rho = 0.92862$, $\dot{\epsilon} = 0.6963$ state using equation (7), shown in figure A-8, clearly overestimates the actual stress obtained.

Also, a maximum in the stress versus time curve for those simulations in the high density/shear rate regime is observed. This indicates that the large shear deformations are producing structural distortions which lag in time somewhat behind the growth of the shear stress but follow rather closely the observed time variation of the normal pressure components in the material. This relatively slower development of what can be thought of as transient stress-induced glide planes is consistent with the observed shear thinning and stress "overshoot" behavior presented. It is also consistent with the observation that the stress relaxation function decays more rapidly in a highly sheared system than in an equilibrium system (see discussion of $g_{\text{eq}}\beta(t)$ above). A comparison of the two types of behavior is presented in figure A-11. The form of these $\phi(t)$ consists of a rapidly ($t < 0.2$) decaying portion which is presumably inertial in origin and due to small motions of the molecules within the random network structure. Further stress relaxation requires the cooperative rearrangement of larger molecular groups and is consequently slower. The attenuation of $\phi(t)$ with increasing shear rate is indicative of the enhanced stress relieving properties of the structurally reorganized system. The stress overshoot observed in nonlinear viscoelastic experiments on polymers has a form that is quite similar to the curves obtained for the LJ system. While the microscopic mechanisms for the two systems are obviously quite different, the general principle that associates the stress overshoot phenomena (as well as shear thinning) with a time dependent structural reorganization process remains quite valid.

In this context it is perhaps relevant to note that a more rapid decay of the stress relaxation function can be thought of as both a suppression of the long relaxation times associated with stress relaxation and also a reduction in the shear rigidity modulus, at low frequencies, G , (a rather well known phenomenon in polymeric systems).*

Thus we see that the viscoelastic studies at high shear rates reflect the structural reorganization that is ultimately responsible for failure or fracture of the liquid. The fact that every property "measured" at high shear rates are found in real and far more complicated liquids suggests strongly that MD studies can be utilized to investigate the comminution process in those liquids.

* Y. G. Yanovski in *Relaxation Phenomena in Polymers*, ed. G. Bartenev and Y. V. Zelenov (Khimiya, Leningrad, 1972), p. 113.

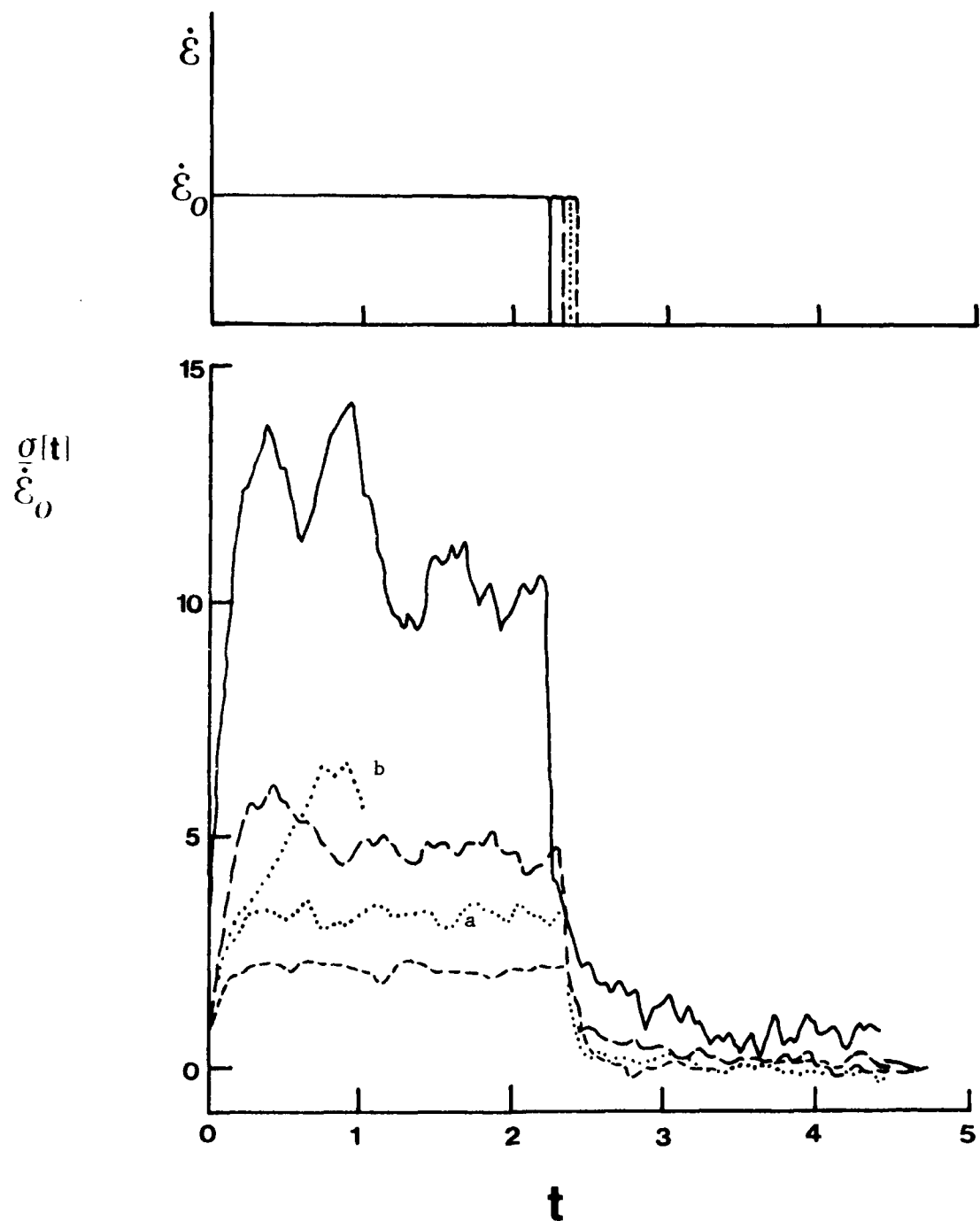


Figure A-8. The Time Dependence of the Reduced Stress, $\sigma(t)/\dot{\epsilon}_0$: $\ldots \rho = 0.8442, \dot{\epsilon}_0 = 0.6745$,
 (a) Actual (b) Predicted Using Equation (4) $\rho = 0.92862, \dot{\epsilon}_0 = 0.6963$;
 $\text{---} \rho = 1.01304, \dot{\epsilon}_0 = 0.7168$; $\text{—} \rho = 1.2663, \dot{\epsilon}_0 = 0.7721$.

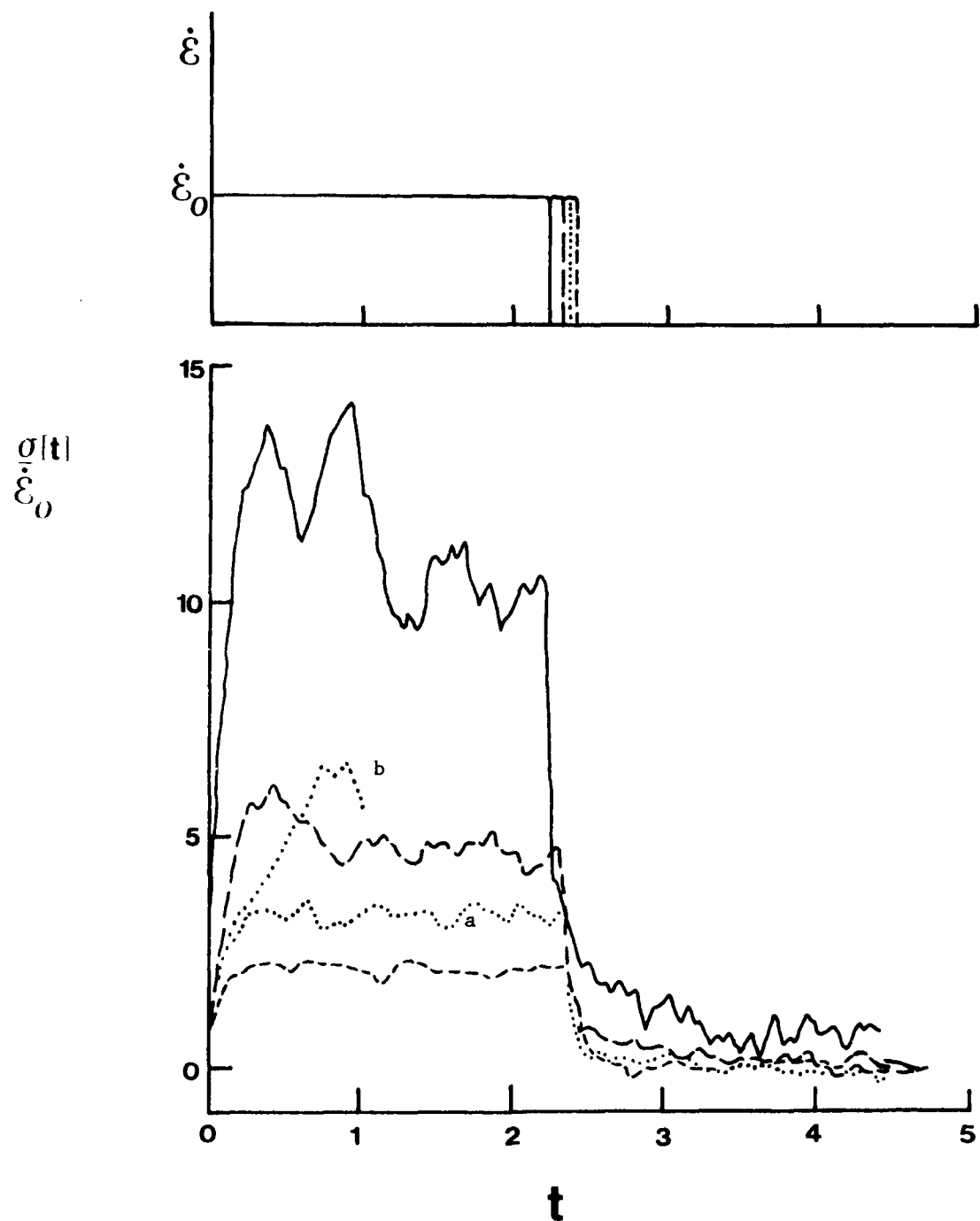


Figure A-8. The Time Dependence of the Reduced Stress, $\sigma(t)/\dot{\epsilon}_0$: $\dots \rho = 0.8442, \dot{\epsilon}_0 = 0.6745$,
 (a) Actual (b) Predicted Using Equation (4) $\rho = 0.92862, \dot{\epsilon}_0 = 0.6963$;
 $\ldots \rho = 1.01304, \dot{\epsilon}_0 = 0.7168$; $__\rho = 1.2663, \dot{\epsilon}_0 = 0.7721$.

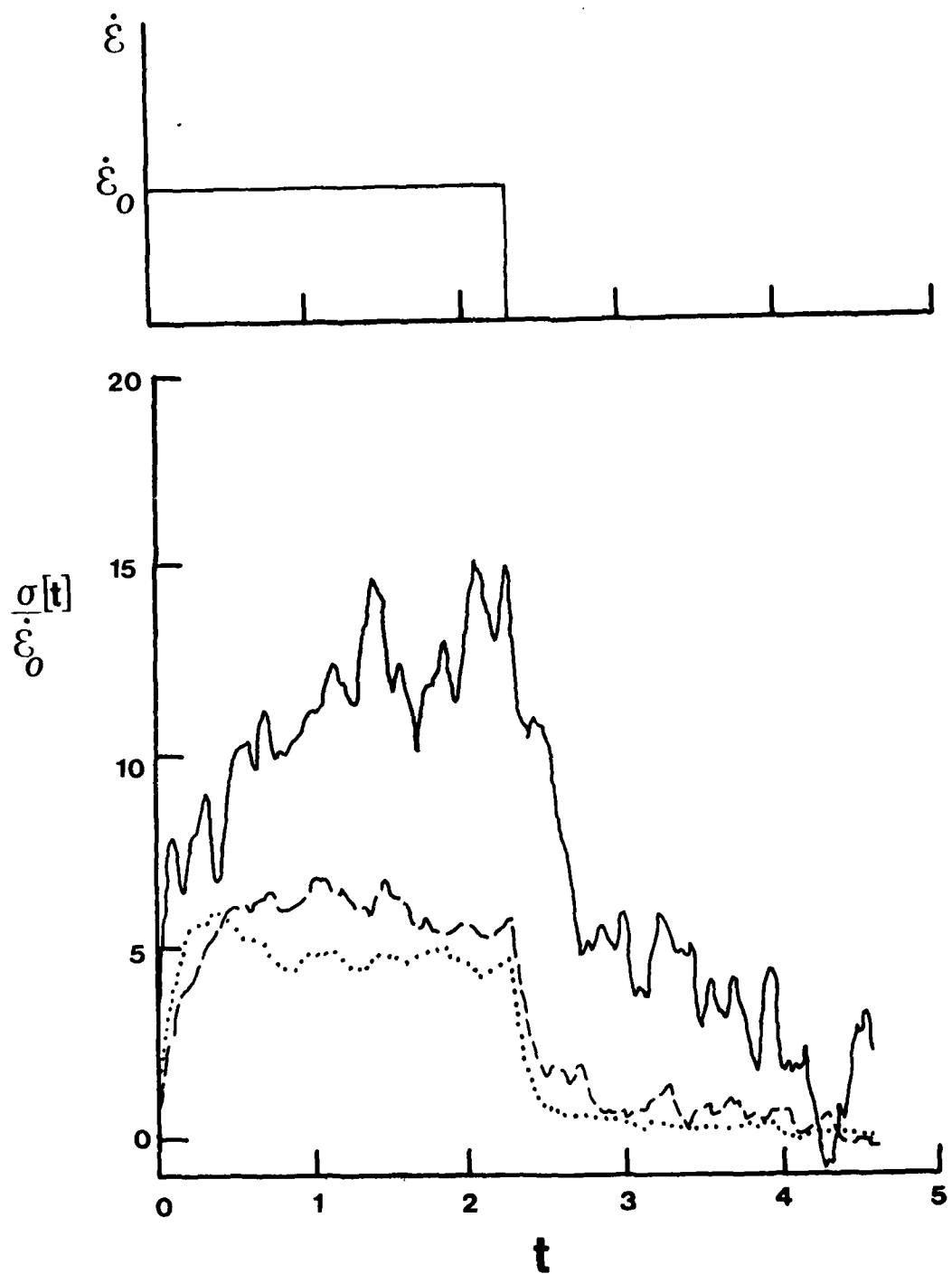


Figure A-9. The Time Dependence of the Reduced Stress, $\sigma(t)/\dot{\epsilon}_0$, for the $p = 1.01304$
State: $\dot{\epsilon}_0 = 0.0896$, $\dot{\epsilon}_0 = 0.3584$, $\dot{\epsilon}_0 = 0.7168$.

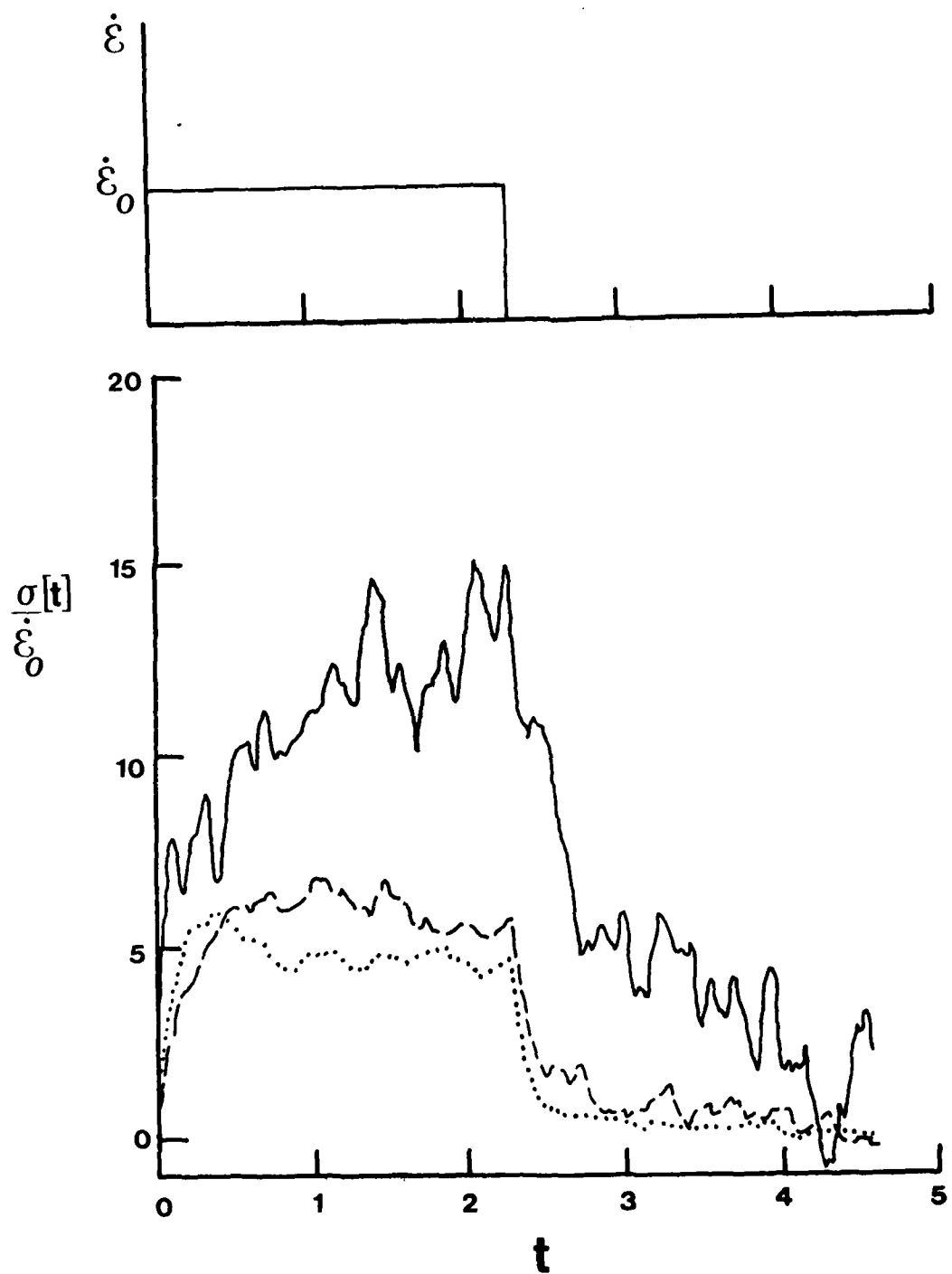


Figure A-9. The Time Dependence of the Reduced Stress, $\sigma(t)/\dot{\epsilon}_0$, for the $p = 1.01304$
State: $\dot{\epsilon}_0 = 0.0896$, $\dot{\epsilon}_0 = 0.3584$, $\dots \dot{\epsilon} = 0.7168$.

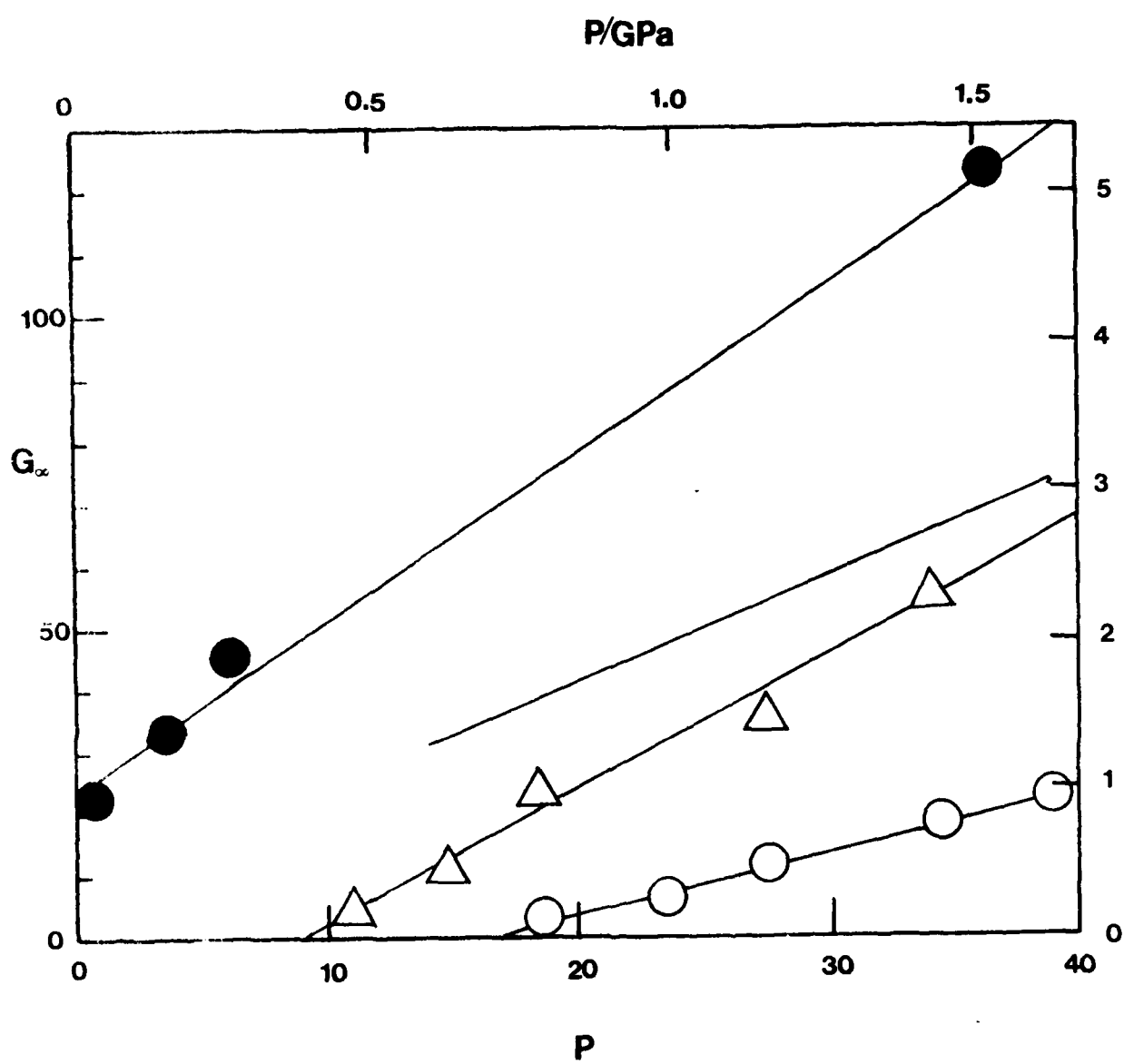


Figure A-10. The Pressure Dependence of G_∞ : Δ Santotrac 40, O Di(2-ethylhexyl) Phthalate from a Twin-Disk Apparatus. Solid line $G_\infty = (0.293 + 1.70P)$ GPa di(2-ethylphthalate. The filled in O is obtained from MHS MD.

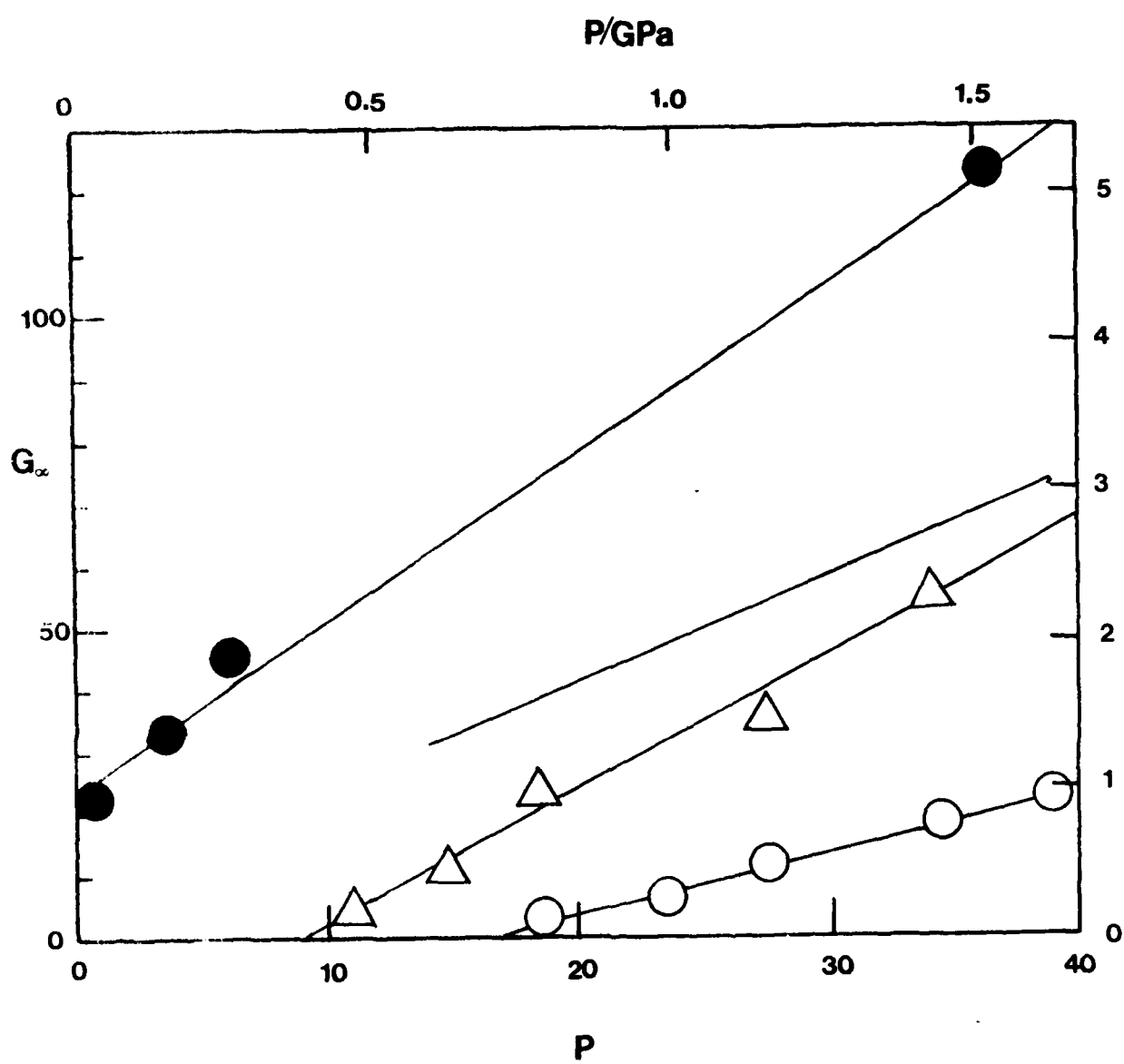


Figure A-10. The Pressure Dependence of G_∞ : Δ Santotrac 40, O Di(2-ethylhexyl) Phthalate from a Twin-Disk Apparatus. Solid line $G_\infty = (0.293 + 1.70P)$ GPa di(2-ethylhexyl) phthalate. The filled in O is obtained from MHS MD.

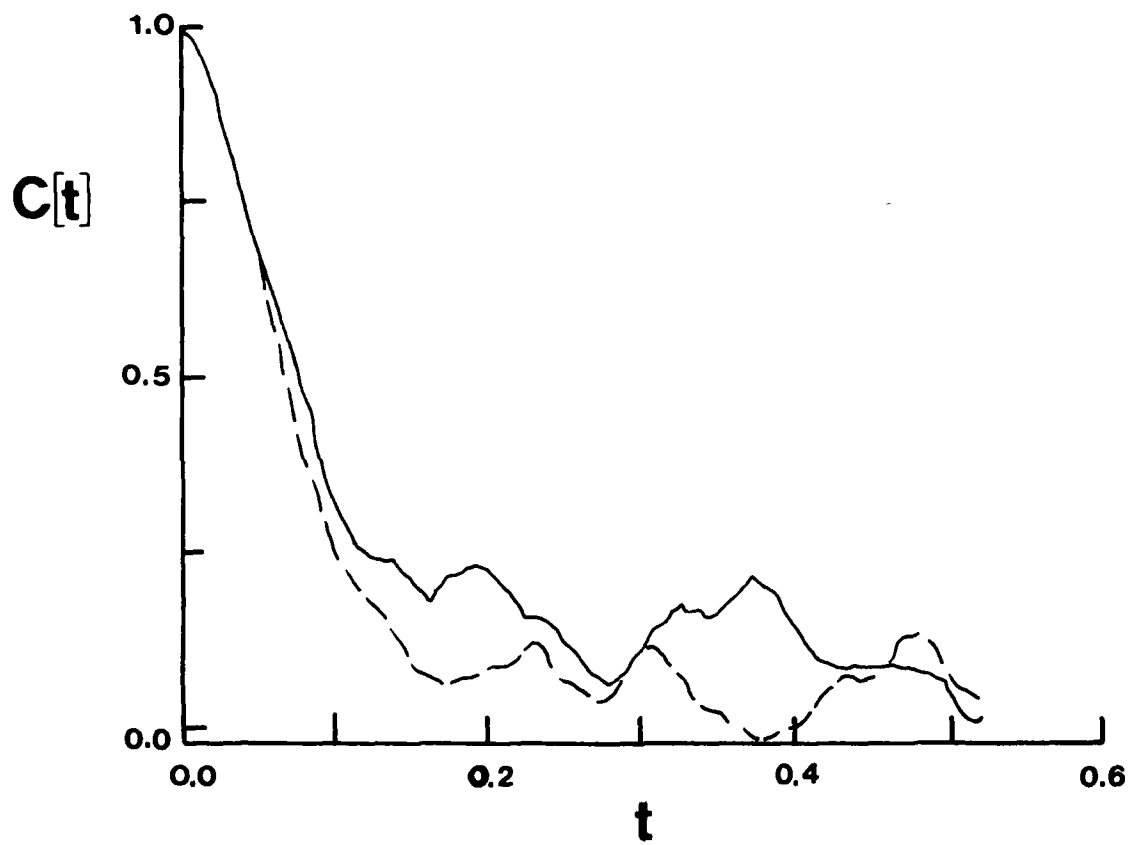
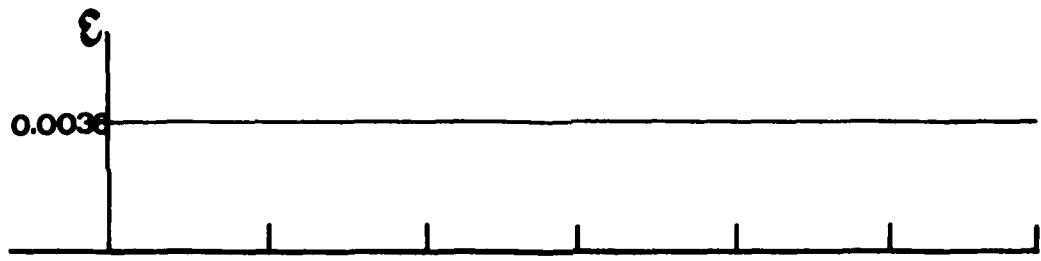


Figure A-11. The Shear Stress Relaxation Functions for the $\rho = 0.8442$ $\dot{\epsilon} = 0$ and $\dot{\epsilon} = 0.6745$. The step in strain ($\dot{\epsilon} = 3.6 \cdot 10^{-3}$) at $t = 0$ is illustrated above this figure.

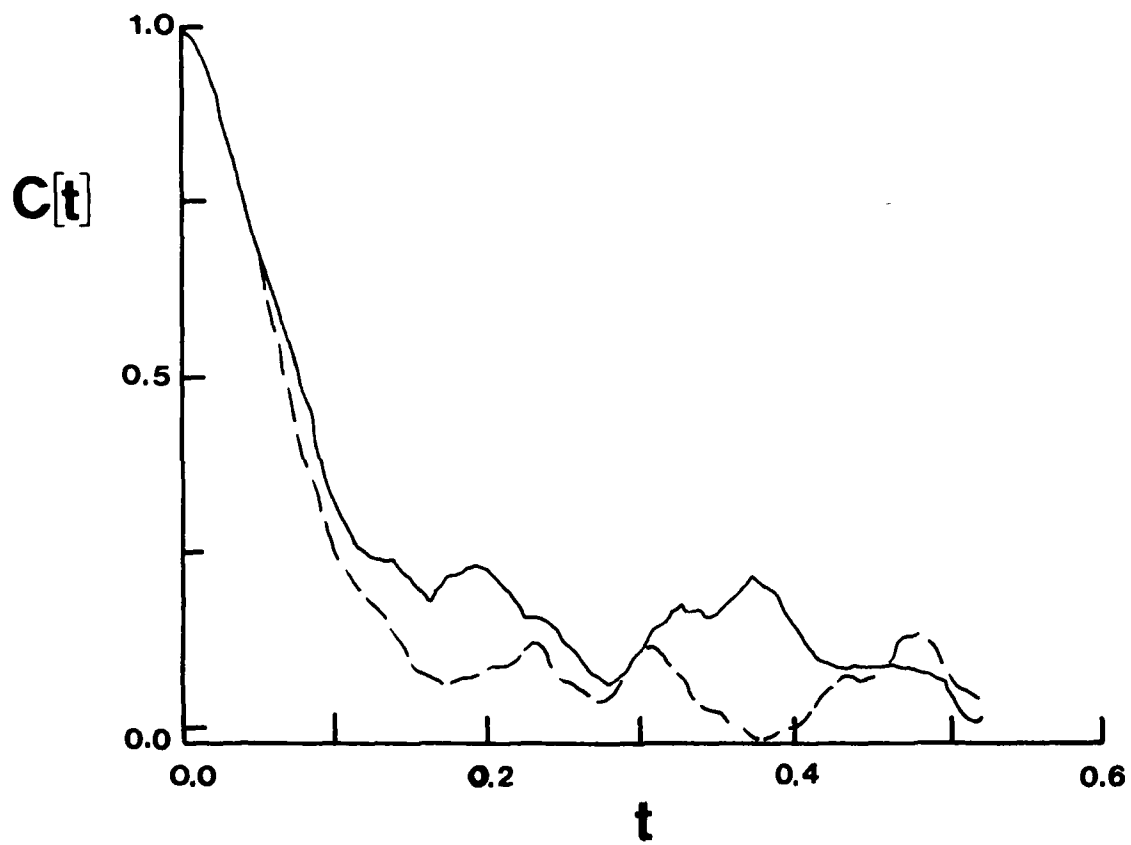
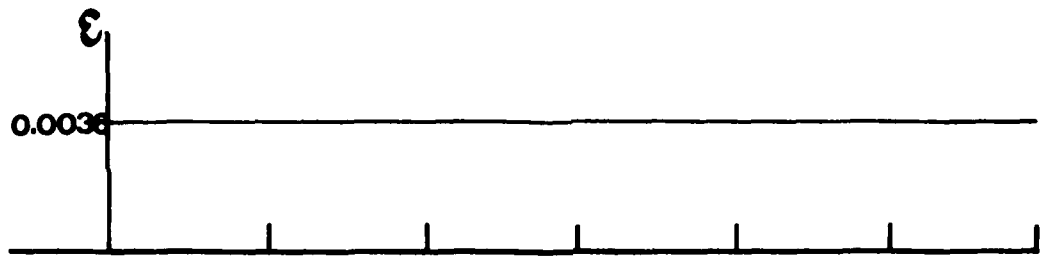


Figure A-11. The Shear Stress Relaxation Functions for the $\rho = 0.8442$ $\dot{\epsilon} = 0$ and $\dot{\epsilon} = 0.6745$. The step in strain ($\dot{\epsilon} = 3.6 \cdot 10^{-3}$) at $t = 0$ is illustrated above this figure.

DISTRIBUTION LIST 2

Names	Copies	Names	Copies
DEPARTMENT OF THE ARMY			
CHEMICAL SYSTEMS LABORATORY			
ATTN: DRDAR-CLF	1	HQDA (DAMO-NCC)	1
ATTN: DRDAR-CLC-B	1	WASH DC 20310	
ATTN: DRDAR-CLC-C	1	HQDA, OCSA	
ATTN: DRDAR-CLC-E	1	ATTN: DACS-FM, MG R. Anson	1
ATTN: DRDAR-CLJ-R	2	Room 1A871, Pentagon	
ATTN: DRDAR-CLJ-L	3	Washington, DC 20310	
ATTN: DRDAR-CLJ-M	1		
ATTN: DRDAR-CLN	1	Federal Emergency Management Agency	
ATTN: DRDAR-CLW	1	Office of Mitigation and Research	
ATTN: DRDAR-CLW-C	1	ATTN: David W. Bensen	1
ATTN: DRDAR-CLW-P	1	Washington, DC 20472	
ATTN: DRDAR-CLW-E	1		
ATTN: DRDAR-CLB-C	1	Deputy Chief of Staff for Research, Development & Acquisition	
ATTN: DRDAR-CLB-P	1	ATTN: DAMA-CSS-C	1
ATTN: DRDAR-CLB-PO	1	ATTN: DAMA-ARZ-D	1
ATTN: DRDAR-CLB-R	1	Washington, DC 20310	
ATTN: DRDAR-CLB-T	1		
ATTN: DRDAR-CLB-TE	1	Department of the Army	
ATTN: DRDAR-CLY-A	1	Headquarters, Sixth US Army	
ATTN: DRDAR-CLY-R	6	ATTN: AFKC-OP-NBC	1
COPIES FOR AUTHOR(S):		Presidio of San Francisco, CA 94129	
Research Division	2		
CLB-A (Record Set)	1	US Army Research and Standardization	
DEPARTMENT OF DEFENSE		Group (Europe)	
Defense Technical Information Center		ATTN: DRXSN-E-SC	1
ATTN: DTIC-DDA-2	12	Box 65, FPO New York 09510	
Cameron Station, Building 5			
Alexandria, VA 22314		HQDA (DAMI-FIT)	1
		WASH, DC 20310	
Director			
Defense Intelligence Agency		Commander	
ATTN: DB-4G1	1	HQ 7th Medical Command	
Washington, DC 20301		ATTN: AEMPM	1
		APO New York 09403	
Special Agent in Charge			
ARO, 902d Military Intelligence GP		Commander	
ATTN: IAGPA-A-AN	1	DARCOM, STITEUR	
Aberdeen Proving Ground, MD 21005		ATTN: DRXST-STI	1
		Box 48, APO New York 09710	
Commander			
SED, HQ, INSCOM		Commander	
ATTN: IRFM-SED (Mr. Joubert)	1	US Army Science & Technology Center-	
Fort Meade, MD 20755		Far East Office	
		ATTN: MAJ Borges	1
		APO San Francisco 96328	

DISTRIBUTION LIST 2

Names	Copies	Names	Copies
DEPARTMENT OF THE ARMY			
CHEMICAL SYSTEMS LABORATORY			
ATTN: DRDAR-CLF	1	HQDA (DAMO-NCC)	1
ATTN: DRDAR-CLC-B	1	WASH DC 20310	
ATTN: DRDAR-CLC-C	1	HQDA, OCSA	
ATTN: DRDAR-CLC-E	1	ATTN: DACS-FM, MG R. Anson	1
ATTN: DRDAR-CLJ-R	2	Room 1A871, Pentagon	
ATTN: DRDAR-CLJ-L	3	Washington, DC 20310	
ATTN: DRDAR-CLJ-M	1		
ATTN: DRDAR-CLN	1	Federal Emergency Management Agency	
ATTN: DRDAR-CLW	1	Office of Mitigation and Research	
ATTN: DRDAR-CLW-C	1	ATTN: David W. Bensen	1
ATTN: DRDAR-CLW-P	1	Washington, DC 20472	
ATTN: DRDAR-CLW-E	1		
ATTN: DRDAR-CLB-C	1	Deputy Chief of Staff for Research, Development & Acquisition	
ATTN: DRDAR-CLB-P	1	ATTN: DAMA-CSS-C	1
ATTN: DRDAR-CLB-PO	1	ATTN: DAMA-ARZ-D	1
ATTN: DRDAR-CLB-R	1	Washington, DC 20310	
ATTN: DRDAR-CLB-T	1		
ATTN: DRDAR-CLB-TE	1	Department of the Army	
ATTN: DRDAR-CLY-A	1	Headquarters, Sixth US Army	
ATTN: DRDAR-CLY-R	6	ATTN: AFKC-OP-NBC	1
COPIES FOR AUTHOR(S):		Presidio of San Francisco, CA 94129	
Research Division	2		
CLB-A (Record Set)	1	US Army Research and Standardization	
DEPARTMENT OF DEFENSE		Group (Europe)	
Defense Technical Information Center		ATTN: DRXSN-E-SC	1
ATTN: DTIC-DDA-2	12	Box 65, FPO New York 09510	
Cameron Station, Building 5			
Alexandria, VA 22314		HQDA (DAMI-FIT)	1
		WASH, DC 20310	
Director			
Defense Intelligence Agency		Commander	
ATTN: DB-4G1	1	HQ 7th Medical Command	
Washington, DC 20301		ATTN: AEMPM	1
		APO New York 09403	
Special Agent in Charge			
ARO, 902d Military Intelligence GP		Commander	
ATTN: IAGPA-A-AN	1	DARCOM, STITEUR	
Aberdeen Proving Ground, MD 21005		ATTN: DRXST-STI	1
		Box 48, APO New York 09710	
Commander			
SED, HQ, INSCOM		Commander	
ATTN: IRFM-SED (Mr. Joubert)	1	US Army Science & Technology Center-	
Fort Meade, MD 20755		Far East Office	
		ATTN: MAJ Borges	1
		APO San Francisco 96328	

Commander 2d Infantry Division ATTN: EAIDCOM APO San Francisco 96224	1	Director Human Engineering Laboratory ATTN: DRXHE-SP (CB Defense Team) Aberdeen Proving Ground, MD 21005	1
Commander 5th Infantry Division (Mech) ATTN: Division Chemical Officer Fort Polk, LA 71459	1	Commander US Army Foreign Science & Technology Center ATTN: DRXST-MT3 220 Seventh St., NE Charlottesville, VA 22901	1
OFFICE OF THE SURGEON GENERAL			
Commander Army Medical Bioengineering Research & Development Laboratory ATTN: SORB-UBD-A Fort Detrick, Bldg 568 Ft. Detrick, MD 21701	1	Director US Army Materiel Systems Analysis Activity ATTN: DRXSY-MP ATTN: DRXSY-TN (Mr. Metz) Aberdeen Proving Ground, MD 21005	1 2
Commanders Army Medical Research and Development Command ATTN: SGMD-PR Fort Detrick, MD 21701	1	Commander US Army Missile Command Redstone Scientific Information Center ATTN: DRSMI-RPR (Documents) Redstone Arsenal, AL 35809	1
Commander Biomedical Laboratory ATTN: SGHD-UV-L Aberdeen Proving Ground, MD 21010	1	Director DARCOM Field Safety Activity ATTN: DRXOS-C Charlestown, IN 47111	1
U.S. ARMY HEALTH SERVICE COMMAND			
Superintendent Academy of Health Sciences US Army ATTN: HSA-CDH ATTN: HSA-IPM Fort Sam Houston, TX 78234	1 1	Commander US Army Natick Research and Development Command ATTN: DRDNA-O ATTN: DRDNA-VC ATTN: DRDNA-VCC ATTN: DRDNA-VM ATTN: DRDNA-VR ATTN: DRDNA-VT Natick, MA 01760	1 1 1 1 1 1
U.S. ARMY MATERIEL DEVELOPMENT AND READINESS COMMAND			
Commander US Army Materiel Development and Readiness Command ATTN: DRCLDC ATTN: DRCSF-P 5000 Eisenhower Ave Alexandria, VA 22353	1 1	US ARMY ARMAMENT RESEARCH AND DEVELOPMENT COMMAND	
Commander US Army Armament Research and Development Command ATTN: DRDAR-LCA-L ATTN: DRDAR-LCU-CE ATTN: DRDAR-PMA (G.R. Sacco) ATTN: DRDAR-SCA-W ATTN: DRDAR-TSS ATTN: DRCPM-CAWS-AM ATTN: DRCPM-CAWS-SI Dover, NJ 07801		Commander US Army Armament Research and Development Command ATTN: DRDAR-LCA-L ATTN: DRDAR-LCU-CE ATTN: DRDAR-PMA (G.R. Sacco) ATTN: DRDAR-SCA-W ATTN: DRDAR-TSS ATTN: DRCPM-CAWS-AM ATTN: DRCPM-CAWS-SI Dover, NJ 07801	1 1 1 1 5 1 1

Commander 2d Infantry Division ATTN: EAIDCOM APO San Francisco 96224	1	Director Human Engineering Laboratory ATTN: DRXHE-SP (CB Defense Team) Aberdeen Proving Ground, MD 21005	1
Commander 5th Infantry Division (Mech) ATTN: Division Chemical Officer Fort Polk, LA 71459	1	Commander US Army Foreign Science & Technology Center ATTN: DRXST-MT3 220 Seventh St., NE Charlottesville, VA 22901	1
OFFICE OF THE SURGEON GENERAL			
Commander Army Medical Bioengineering Research & Development Laboratory ATTN: SORB-UBD-A Fort Detrick, Bldg 568 Ft. Detrick, MD 21701	1	Director US Army Materiel Systems Analysis Activity ATTN: DRXSY-MP ATTN: DRXSY-TN (Mr. Metz) Aberdeen Proving Ground, MD 21005	1 2
Commanders Army Medical Research and Development Command ATTN: SGMD-PR Fort Detrick, MD 21701	1	Commander US Army Missile Command Redstone Scientific Information Center ATTN: DRSMI-RPR (Documents) Redstone Arsenal, AL 35809	1
Commander Biomedical Laboratory ATTN: SGHD-UV-L Aberdeen Proving Ground, MD 21010	1	Director DARCOM Field Safety Activity ATTN: DRXOS-C Charlestown, IN 47111	1
U.S. ARMY HEALTH SERVICE COMMAND			
Superintendent Academy of Health Sciences US Army ATTN: HSA-CDH ATTN: HSA-IPM Fort Sam Houston, TX 78234	1 1	Commander US Army Natick Research and Development Command ATTN: DRDNA-O ATTN: DRDNA-VC ATTN: DRDNA-VCC ATTN: DRDNA-VM ATTN: DRDNA-VR ATTN: DRDNA-VT Natick, MA 01760	1 1 1 1 1 1
U.S. ARMY MATERIEL DEVELOPMENT AND READINESS COMMAND			
Commander US Army Materiel Development and Readiness Command ATTN: DRCLDC ATTN: DRCSF-P 5000 Eisenhower Ave Alexandria, VA 22353	1 1	US ARMY ARMAMENT RESEARCH AND DEVELOPMENT COMMAND	
Commander US Army Armament Research and Development Command ATTN: DRDAR-LCA-L ATTN: DRDAR-LCU-CE ATTN: DRDAR-PMA (G.R. Sacco) ATTN: DRDAR-SCA-W ATTN: DRDAR-TSS ATTN: DRCPM-CAWS-AM ATTN: DRCPM-CAWS-SI Dover, NJ 07801		Commander US Army Armament Research and Development Command ATTN: DRDAR-LCA-L ATTN: DRDAR-LCU-CE ATTN: DRDAR-PMA (G.R. Sacco) ATTN: DRDAR-SCA-W ATTN: DRDAR-TSS ATTN: DRCPM-CAWS-AM ATTN: DRCPM-CAWS-SI Dover, NJ 07801	1 1 1 1 5 1 1

US ARMY ARMAMENT MATERIEL READINESS COMMAND	Commander USA Combined Arms Center and Fort Leavenworth ATTN: ATZL-CA-COG 1 ATTN: ATZL-CAM-IM 1 Fort Leavenworth, KS 66027
Commander US Army Armament Materiel Readiness Command ATTN: DRSAR-ASN 1 ATTN: DRSAR-SF 1 ATTN: DRSAR-SR 1 Rock Island, IL 61299	Commander US Army TRADOC System Analysis Activity 1 ATTN: ATAA-SL White Sands Missile Range, NM 88002
Commander USA ARRCOM ATTN: SART 1 Aberdeen Proving Ground, MD 21010	US ARMY TEST & EVALUATION COMMAND
Commander US Army Dugway Proving Ground ATTN: Technical Library (Docu Sect) 1 Dugway, UT 84022	Commander US Army Test & Evaluation Command ATTN: DRSTE-CT-T 1 Aberdeen Proving Ground, MD 21005
US ARMY TRAINING & DOCTRINE COMMAND	DEPARTMENT OF THE NAVY
Commandant US Army Infantry School ATTN: NBC Division 1 Fort Benning, GA 31905	Chief of Naval Research ATTN: Code 443 1 800 N. Quincy Street Arlington, VA 22217
Commandant US Army Missile & Munitions Center and School ATTN: ATSK-DT-MU-EOD 1 Restone Arsenal, AL 35809	Commander Naval Explosive Ordnance Disposal Facility ATTN: Army Chemical Officer (Code AC-3) 1 Indian Head, MD 20640
Commandant USAMP&CS/TC&FM ATTN: ATZN-CM-CDM 1 Fort McClellan, AL 36205	Commander Naval Surface Weapons Center Code G51 1 Dahlgren, VA 22448
Commander US Army Infantry Center ATTN: ATSH-CD-MS-C 1 Fort Benning, GA 31905	Chief, Bureau of Medicine & Surgery Department of the Navy ATTN: MED 3C33 1 Washington, DC 20372
Commander US Army Infantry Center Directorate of Plans & Training ATTN: ATZB-DPT-PO-NBC 1 Fort Benning, GA 31905	Commander Naval Weapons Center ATTN: Technical Library (Code 343) 1 China Lake, CA 93555
Commander USA Training and Doctrine Command ATTN: ATCD-Z 1 Fort Monroe, VA 23651	US MARINE CORPS
	Director, Development Center Marine Corps Development and Education Command ATTN: Fire Power Division 1 Quantico, VA 22134

US ARMY ARMAMENT MATERIEL READINESS COMMAND	Commander USA Combined Arms Center and Fort Leavenworth ATTN: ATZL-CA-COG 1 ATTN: ATZL-CAM-IM 1 Fort Leavenworth, KS 66027
Commander US Army Armament Materiel Readiness Command ATTN: DRSAR-ASN 1 ATTN: DRSAR-SF 1 ATTN: DRSAR-SR 1 Rock Island, IL 61299	Commander US Army TRADOC System Analysis Activity 1 ATTN: ATAA-SL White Sands Missile Range, NM 88002
Commander USA ARRCOM ATTN: SART 1 Aberdeen Proving Ground, MD 21010	US ARMY TEST & EVALUATION COMMAND
Commander US Army Dugway Proving Ground ATTN: Technical Library (Docu Sect) 1 Dugway, UT 84022	Commander US Army Test & Evaluation Command ATTN: DRSTE-CT-T 1 Aberdeen Proving Ground, MD 21005
US ARMY TRAINING & DOCTRINE COMMAND	DEPARTMENT OF THE NAVY
Commandant US Army Infantry School ATTN: NBC Division 1 Fort Benning, GA 31905	Chief of Naval Research ATTN: Code 443 1 800 N. Quincy Street Arlington, VA 22217
Commandant US Army Missile & Munitions Center and School ATTN: ATSK-DT-MU-EOD 1 Restone Arsenal, AL 35809	Commander Naval Explosive Ordnance Disposal Facility ATTN: Army Chemical Officer (Code AC-3) 1 Indian Head, MD 20640
Commandant USAMP&CS/TC&FM ATTN: ATZN-CM-CDM 1 Fort McClellan, AL 36205	Commander Naval Surface Weapons Center Code G51 1 Dahlgren, VA 22448
Commander US Army Infantry Center ATTN: ATSH-CD-MS-C 1 Fort Benning, GA 31905	Chief, Bureau of Medicine & Surgery Department of the Navy ATTN: MED 3C33 1 Washington, DC 20372
Commander US Army Infantry Center Directorate of Plans & Training ATTN: ATZB-DPT-PO-NBC 1 Fort Benning, GA 31905	Commander Naval Weapons Center ATTN: Technical Library (Code 343) 1 China Lake, CA 93555
Commander USA Training and Doctrine Command ATTN: ATCD-Z 1 Fort Monroe, VA 23651	US MARINE CORPS
	Director, Development Center Marine Corps Development and Education Command ATTN: Fire Power Division 1 Quantico, VA 22134

DEPARTMENT OF THE AIR FORCE

HQ Foreign Technology Division (AFSC)
ATTN: TQTR
Wright-Patterson AFB, OH 45433

1

Commander
Aeronautical Systems Division
ATTN: ASD/AELD
ATTN: ASD/AESD
Wright-Patterson AFB, OH 45433

1

HQ AFLC/LOWMM
Wright-Patterson AFB, OH 45433

1

HQ, AFSC/SDNE
Andrews AFB, MD 20334

1

HQ AMD/RD
ATTN: Chemical Defense OPR
Brooks AFB, TX 78235

1

NORAD Combat Operations Center
ATTN: DOUN
Cheyenne Mtn Complex, CO 80914

1

Air Force Aerospace Medical Research
Laboratory
ATTN: AFAMRL/HE (Dr. C.R. Reigle)
Wright-Patterson AFB, OH 45433

1

HQ AFTEC/SGB
Kirtland AFB, NM 87117

1

OUTSIDE AGENCIES

Battelle, Columbus Laboratories
ATTN: TACTEC
505 King Avenue
Columbus, OH 43201

1

Toxicology Information Center, WG 1008
National Research Council
2101 Constitution Ave., NW
Washington, DC 20418

1

US Public Health Service
Center for Disease Control
ATTN: Lewis Webb, Jr.
Building 4, Room 232
Atlanta, GA 30333

1

DEPARTMENT OF THE AIR FORCE

HQ Foreign Technology Division (AFSC)
ATTN: TQTR
Wright-Patterson AFB, OH 45433

1

Commander
Aeronautical Systems Division
ATTN: ASD/AELD
ATTN: ASD/AESD
Wright-Patterson AFB, OH 45433

1

HQ AFLC/LOWMM
Wright-Patterson AFB, OH 45433

1

HQ, AFSC/SDNE
Andrews AFB, MD 20334

1

HQ AMD/RD
ATTN: Chemical Defense OPR
Brooks AFB, TX 78235

1

NORAD Combat Operations Center
ATTN: DOUN
Cheyenne Mtn Complex, CO 80914

1

Air Force Aerospace Medical Research
Laboratory
ATTN: AFAMRL/HE (Dr. C.R. Reigle)
Wright-Patterson AFB, OH 45433

1

HQ AFTEC/SGB
Kirtland AFB, NM 87117

1

OUTSIDE AGENCIES

Battelle, Columbus Laboratories
ATTN: TACTEC
505 King Avenue
Columbus, OH 43201

1

Toxicology Information Center, WG 1008
National Research Council
2101 Constitution Ave., NW
Washington, DC 20418

1

US Public Health Service
Center for Disease Control
ATTN: Lewis Webb, Jr.
Building 4, Room 232
Atlanta, GA 30333

1

